SBIR-08.10-5433
release date 4/09/91 ✓

Dynamics Technology, Inc.

DT-8619-89007

FIBER-OPTIC THREE AXIS MAGNETOMER

PROTOTYPE DEVELOPMENT

OCTOBER 1989

PREPARED BY: THOMAS D. WANG
DAVID G. McCOMB
BRADLEY R. KINGSTON
C. MICHAEL DUBE
KENNETH A. POEHLS
KEITH WANSER

SUBMITTED TO: NATIONAL AERONAUTICS AND SPACE ADMINISTRATION
RESIDENT OFFICE - JET PROPULSION LABORATORY
4800 OAK GROVE DRIVE
PASADENA, CA 91109

Dynamics Technology, Inc.
21311 Hawthorne Blvd.
Suite 300
Torrance, CA 90503
(213) 543-5433

PROJECT SUMMARY

The goal of this research program was to develop a high sensitivity, fiber optic, interferometric, three-axis magnetometer for interplanetary spacecraft applications. Dynamics Technology, Inc. (DTI) has successfully integrated a low noise, high bandwidth interferometer with high sensitivity metallic glass transducers. Also, DTI has developed sophisticated signal processing electronics and complete data acquisition, filtering, and display software. The sensor was packaged in a compact, low power and weight unit which facilitates deployment. The magnetic field sensor had subgamma sensitivity and a dynamic range of 10^5 gamma in a 10 Hz bandwidth.

Furthermore, the vector instrument exhibited the lowest noise level when only one axis was in operation. A system noise level of 1 gamma rms was observed in a 1 Hz bandwidth. However, with the other two channels operating, the noise level increased by about one order of magnitude. Higher system noise was attributed to cross-channel interference among the dither fields.

FOREWORD

This report documents the results of a Phase II SBIR program to develop a fiber optic magnetometer. This work was performed under NASA Contract No. NAS7-1001, and the technical monitor was Dr. Roy Marquedant.

Table of Contents

1.0 INTRODUCTION

Measurements of planetary magnetic fields require a sensor system with a dynamic range of approximately 10^{-3} to 10^{5} gammas and a bandwidth of 1 to 100 Hz. While the large fields can be measured with a small solid state sensor (e.g., a Hall effect device), measurement of the low fields requires a more sophisticated sensor. Vector field measurements impose additional sensor complexity. However, for spacecraft applications, such high resolution sensors can carry a significant weight, volume, or power penalty. Ideally, one would prefer a single, compact, low power mangetic sensor with high sensitivity and a very large dynamic range (~ 160 dB).

Two types of magnetometers have been utilized in recent interplanetary space exploration missions: the ring core fluxgate magnetometer (FGM) and the optically pumped vector helium magnetometer (VHM). State-of-the-art implementations of both devices have achieved sensitivity of approximately 0.01 nT at 1 Hz. The VHM is generally agreed to have better sensitivity and stability than the FGM; however, the VHM is noise limited to a bandwidth of 1 Hz or less. For frequencies greater than 1 Hz, the FGM is successfully used even though the slow drift of the zero level offset is unavoidable and necessitates the use of a mechanical flipper to quickly rotate the sensor 180° for inflight calibration. Thus, for missions in which magnetic measurements of both low frequency (for planetary magnetic field and geologic anomalies) and high frequency (for solar wind interaction) are desired, two magnetometer systems have been deployed.

A fiber optic magnetometer is an attractive candidate for future spacecraft-based planetary magnetic field measurements. Its key potential features are:

- Small size and light weight
- High sensitivity
- Large dynamic range

- Versatile geometric configuration
- Vector or total field capability
- Small gradiometer baseline
- Large bandwidth

The goal of this SBIR research program was to build and test a fiber optic magnetometer with both high sensitivity and large dynamic range over a wide bandwidth. The design goals and measured performance for the three-axis sensor are shown in Table 1.1.

TABLE 1.1 FIBER OPTIC MAGNETOMETER DESIGN GOALS AND CURRENT PERFORMANCE

	GOAL	MEASURED
Sensitivity	10^{-3} gamma (vector field)	0.3 gamma
Range	10^{-3} - 10^{5} gamma	0.3 - 10^{5} gamma
Bandwidth	$\gtrsim$ 10 Hz	100 Hz
Power Consumption	1-3 watts	35 watts
Weight	1-2 kg	8 kg
Environment:		
Temperature	-40°C to +40°C (During Transit)	Not Tested
	±10°C of design point (During Operation)	±10°C
Radiation	50 krad	Not Tested
Offset Stability	0.1 gamma/°C	Not Tested

This program required systematic development of high sensitivity magnetostrictive transducer materials, high resolution and high bandwidth optical interferometry, low noise electronic circuitry, dual feedback control loop design, data acquisition and system control software, and mechanical packaging design. DTI has addressed each of these issues in a balanced program, and has successfully produced a working three axis magnetometer.

During the contract period, DTI has completed the following tasks:

- Increased transducer sensitivity
- Measured transverse field sensitivity
- Reduced system noise and drift
- Implemented laser thermal stabilization circuit
- Reduced power consumption
- Reduced breadboard electronics to pcb
- Developed data collection, filtering, and display software
- Conducted lab tests
- Analyzed magnetometer signature, drift, and noise level
- Measured cross-talk among channels

This report provides a detailed summary of the design and testing of the Phase II prototype sensor. The system design concept and analysis is discussed in Section 2, and the hardware implementation and assembly is detailed in Sections 3-5. Instrument operational procedures are described in Section 6, and the results of the Phase II laboratory tests are presented in Section 7. Section 8 contains an extended discussion of the noise sources encountered and approaches to their resolution. Some brief recommendations for future research are summarized in Section 9.

2.0 SENSOR SYSTEM DESIGN

The DTI interferometetric three axis sensor consists of three fiber optic magnetometer channels positioned in orthogonal directions. Each fiber optic magnetometer is composed of a dual, coupled control system which produces a linear and stable measurement of the total magnetic field at the transducer. The coupled control loops are referred to as the optical feedback loop and the magnetic feedback loop.

The system design consisted of placing the x and y axes magnetometers on one interferometer, and locating the z axis magnetometer on a second one. The sensor configuration is shown in Figure 2.1. The three channels were separated onto two sensor systems rather than one to reduce cross-talk between the dither frequencies. Less cross-channel interference would be attained by placing each channel on its own separate interferometer; however, the laser did not have enough light power to transmit light through the fiber on three interferometers.

To achieve the desired magnetic sensitivity, it is necessary to have a highly stable and linear fiber optic Mach-Zehnder interferometer capable of measuring 10^{-5} radian or lower signals in a field environment. In order to achieve this performance level, the interferometer was operated in the so-called "high gain bandwidth" active homodyne mode in which the interferometer is continuously maintained near balance; i.e. the outputs of the two signal legs are kept equal for maximum sensitivity and linearity. A signal processing scheme utilizing the quadratic response of the magnetostrictive transducers shifts up in frequency interferometer signals representing sensed low frequency magnetic fields, bypassing 1/f low frequency system noise. Demodulated transducer output is integrated and fed back to the magnetic transducers, holding the total field constant, providing a linear measure of sensed magnetic field and eliminating hysteresis difficulties. The following section describes the design of the fiber optic interferometer and is followed by a section discussing the magnetic feedback control loop analysis and design.

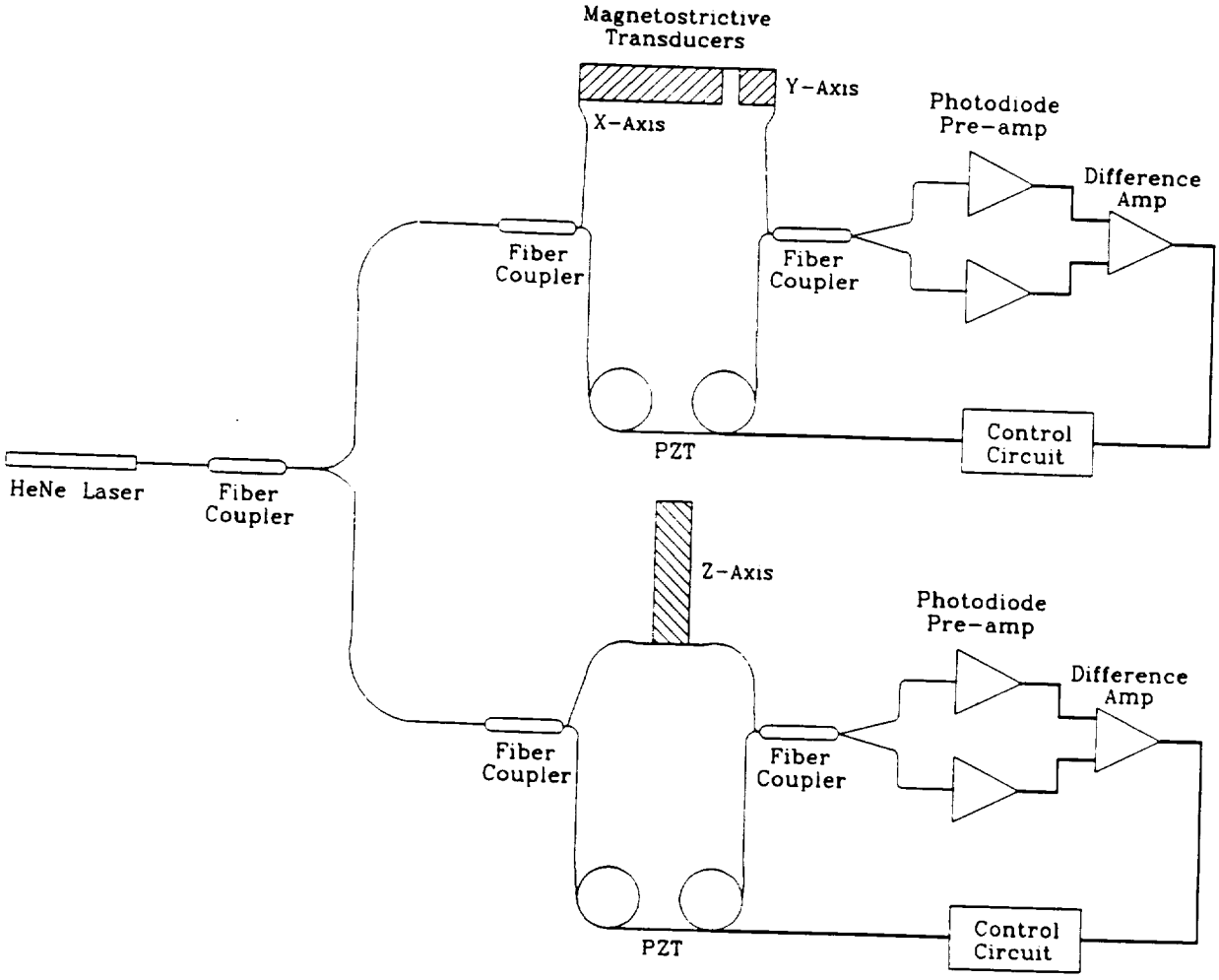

Figure 2.1 Fiber Optic Mach Zehnder Interferometer System used as a Three-axis Magnetometer Sensor.

2.1 Fiber Optic Mach-Zehnder Interferometry

The basic fiber optic magnetometer is built upon a Mach-Zehnder interferometer, a well established approach in fiber sensor research. The theoretical performance levels of a Mach-Zehnder are displayed in Table 2.1. Light is coupled via an integrated fiber optic directional coupler (i.e., a beamsplitter) from a He-Ne laser source into two single mode optical fibers that comprise the two legs of the interferometer.

In the signal leg, the fiber is attached to a magnetostrictive material (e.g., metallic glass) which strains the fiber, causing a change in optical path length proportional to the square of the applied magnetic field. The light in the two legs is recombined in a second coupler, producing a distribution of intensity in the two output fibers that depends on the relative phase difference of the light in each leg. The induced phase shift is detected by a pair of photodiodes as an output intensity change. The compensator circuitry and the piezoelectric cylinders (PZT's) are used in an active feedback loop to maintain the interferometer in "quadrature" as described below.

In general, the light output of a fiber interferometer can be split in any proportion between the two output fibers, depending on the relative phase at the output coupler as shown in Figure 2.2. The interferometer is most sensitive to small phase changes when the relative phase in the two optical legs is $\pi/2$, $3\pi/2$, etc. This situation, called the "quadrature condition," occurs when the two output fibers have equal intensity. In general, slow ambient temperature variations will cause substantial drift in the relative output phase due to minute differential strains in the two interferometer legs. One technique to maintain the interferometer in the quadrature condition is to use a compensator circuit and an opto-mechanical phase shifter in a feedback loop. Piezoelectric materials are known to have linear voltage-expansion coefficients in the angstrom range; thus, they were used here to strain the fiber in the interferometer legs.

TABLE 2.1 MACH-ZEHNDER INTERFEROMETER THEORETICAL PERFORMANCE

NOMINAL PERFORMANCE LEVELS		LIMITING FACTORS
• MIN DETECTABLE PHASE SHIFT:	1 μrad/$\sqrt{Hz}$ AT 1 kHz (PER MM PATH MISMATCH)	• LASER FREQ NOISE $f^{-1/2}$
• SINGLE DYNAMIC RANGE:	$\sim 10^6$ IN 1 Hz BAND (0.5% THD)	• DEMODULATION ELECTRONICS SATURATION
• SIGNAL FREQUENCY RESPONSE:	~DC TO 50 MHz ~5 Hz TO 100 kHz	• DETECTOR BANDWIDTH • REDUCED TO PRACTICE
• ENVIRONMENTAL STABILITY:	<5% SCALE FACTOR ERROR (~ 20 dB AGC)	• TEMP/PRESSURE EFFECTS — POLARIZATION FADING — ELECTRONIC DRIFTS — LASER FREQUENCY SHIFTS — F.O. COMPONENT DRIFTS — LASER COUPLING
• LOW FREQUENCY RESPONSE:	$f \gtrsim 5$ Hz	• BACKGROUND — TEMPERATURE — VIBRATION — ACOUSTIC/PRESSURE — MAGNETIC FIELD — ELECTRIC FIELD

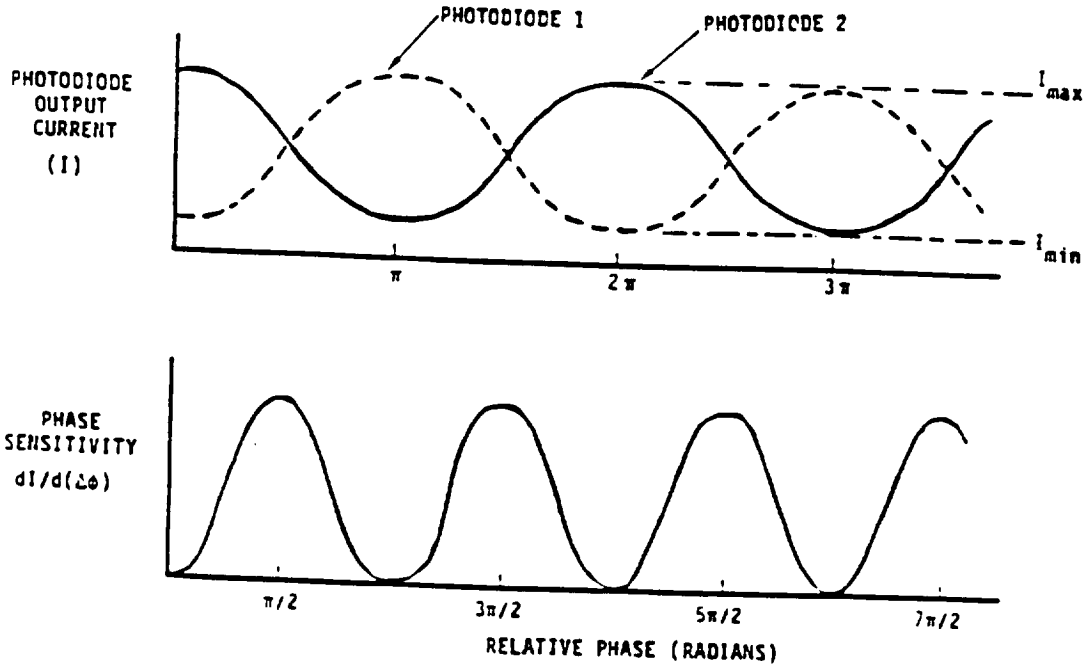

Figure 2.2 Interferometer Phase Sensitivity

Fiber optic directional couplers distribute energy between two or more fibers. In a fiber interferometer, couplers perform the same function as beam splitters in a bulk optic interferometer. Evanescent coupling occurs when fiber cores are sufficiently close for their energy distribution to overlap. The coupling ratio, which is laser frequency dependent, is adjusted by varying the length and degree of field overlap. The coupler must be ruggedized to insure constant coupling with temperature variations. The 2 x 2 (2 input fibers, 2 output fibers) 3 dB couplers used for the interferometer have only become commercially available in the last few years.

For efficient interferometric coupling (i.e., optimum constructive and destructive interference), the light in each leg must have the same polarization direction at the output coupler. Although the light output of a laser may be highly polarized, small birefringence in single mode fibers significantly alters this polarization. Differences in polarization result in a reduction of the fringe visibility. Drifting of the polarization with time will change the fringe visibility and, therefore, the phase sensitivity of the device.

In order to minimize the polarization drift problem, a phase detection scheme was used that minimizes the polarization drift effect with a fast quadrature tracking feedback loop that keeps the photodiode output levels equal, irrespective of the fringe visibility. A discussion of polarization fade effects on system sensitivity and signal-to-noise ratio is discussed in Section 8.3. In this scheme, an optical "error signal" generated in the interferometer by either signal or noise is filtered, integrated and then fed back to two fiber wound piezoelectric control elements, keeping the interferometer balanced. The integrated error signal is then a linear measure of optical phase shift to be evaluated. The control circuitry has a bandwidth near 3 KHz, with signals of less than 3 KHz fed back with a large tracking range piezoelectric element (~700 radians). Thus, large, low frequency acoustical and thermal noise can be tracked for long periods without need for integrator resets; and a high volts/radian calibration can be maintained for signals at the carrier frequencies for precise signal measurement. This approach has several key advantages for the fiber optic magnetometer application:

- The calibration of optical phase shift depends only on the fixed piezoelectric strain constant of the feedback element. It is nominally insensitive to polarization drift which affects fringe visibility. In this technique the principal effect of polarization drift is to partially reduce the sensor bandwidth, a problem that can be largely overcome by conservative design of the feedback bandwidth.

- The interferometer can track linearly over a large range of optical phase shift. The metallic glass transducer exhibits a large signal at the second harmonic of the dither frequency even when the DC field is nulled. If, for example a 10^{-2} gamma field is equivalent to 10^{-5} radians, then a 0.1 Gauss dither field will generate a roughly 10 radian optical phase shift. This second harmonic must be tracked with sufficient resolution to keep the interferometer error signal on the acceptably linear part of the interference fringe ($\lesssim 10^{-2}$ radian offset from balance). This range of acceptable offset is determined by computing the third harmonic contribution of the basic sinusoidal interferometer output, mixing it with the large second harmonic signal, and calculating the "mixed component" at the fundamental dither frequency which constitutes a noise source in the DC field measurement.

The requirements for high frequency and large dynamic range, together with characteristic mechanical resonances and piezoelectric strain response, dictate a carefully integrated interferometer control circuit design. The DTI circuit is configured as a second order feedback circuit. The circuit characteristics were modeled with a PC-based code developed at DTI that allowed us to optimize performance and isolate control circuit features from magnetic and optical effects.

An important constraint in the circuit design is the need to prevent the fundamental mechanical resonance of the piezoelectric element from causing loop instability, as indicated by the requirement that the open loop gain be less than one at the resonant frequency. Careful measurements of the piezoelectric element's resonant frequency and Q were made to support this analysis.

2.2 Dual-Coupled Feedback Loop Design

The DTI fiber optic magnetometer consists of two coupled control loops. The optical control system is used to hold a Mach-Zehnder interferometer in a quadrature condition and to provide a modulated signal whose amplitude is proportional to ambient magnetic fields. A second control system demodulates the optical signal utilizing it to apply magnetic feedback, nulling the field at the magnetic transducers. The magnetic feedback thus provides a measure of the sensed field.

DTI used the so-called closed-loop magnetometer scheme to insure accurate scale factor calibration and to eliminate transducer magnetic hysteresis. A more complete discussion of control loops appears in Section 2.4.

The closed loop has a number of advantages over the open loop technique originally planned. Our analysis of the coupled feedback loop equations has shown that when

the gain of the magnetic feedback loop is much greater than the gain of the optical interferometer loop, the sensed magnetic field, as measured by the feedback voltage to the nulling coil, is independent of the transducer sensitivity coefficient, feedback gains, etc., and depends only on the Oersted/Volt conversion coefficient of the nulling coil. This allows one to balance the three magnetometers fairly precisely to begin with, simply by matching the coil geometries. This is a much better balance (to at least one part in a hundred based on dimensional tolerances) than can be obtained by directly matching the transducers, due to differences in construction variables such as bonding stress, annealing temperature, etc.

Another advantage of the closed loop technique is that it allows a much greater dynamic range DC field. This is in contrast to the open loop case, which allows the transducer to become partially saturated in ambient fields above a few tenths of a gauss.

A crucial assumption of the magnetic feedback scheme is that the transducer response is only along its axis and not perpendicular to its axis, otherwise a multiaxis nulling field must be applied to compensate for the transverse response. For reasonably long, thin transducers, (4 to 1 aspect ratio) we have found the transverse response to be less than 1 percent of the longitudinal response with a longitudinal dither field.

2.3 Transducer Design

The metallic glass transducer has a quadratic strain response to applied magnetic fields up to 0.5 gauss, as shown in Figure 2.3.

$$\epsilon = CH_a^2 \qquad (2.1)$$

where ϵ = magnetostrictive strain,
C = material sensitivity coefficient,
H_a = applied magnetic field.

The development and annealing of the metallic glass transducer is discussed in Appendix I. Low frequency thermal and acoustic noise are avoided by shifting the signal of interest up to higher frequencies. This result is accomplished by dithering the sensor with a magnetic field $H_{\omega i}$ around 10 KHz,

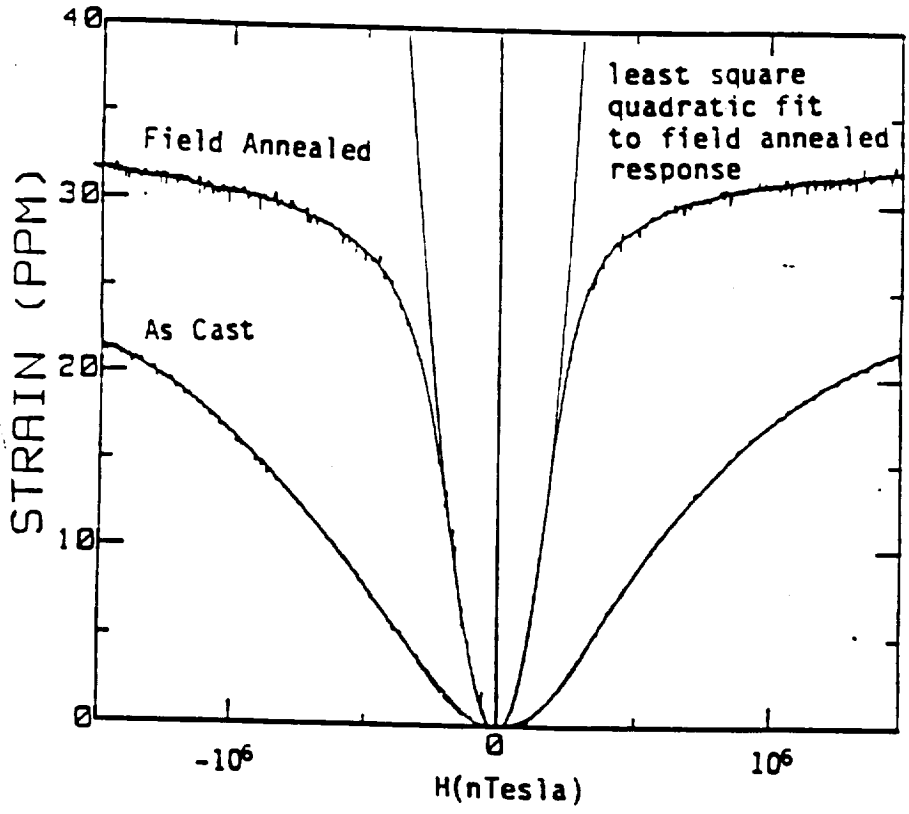

Figure 2.3 Applied D.C. Field

$$H_{\omega_i}(t) = H_i \sin \omega_i t \qquad (2.2)$$

where H_i = peak amplitude; for i = x, y, and z

ω_i = angular frequency.

When the dither H_{ω_i} and low frequency signal field H_s are combined,

$$H_a = H_{\omega_i} + H_s \qquad (2.3)$$

the transducer response contains three terms,

$$\epsilon = C\,(H_s^2 + 2H_{\omega_i} H_s + H_{\omega_i}^2) \qquad (2.4)$$

The dc term is mixed with low frequency noise; thus, signal field H_s can be better measured with a narrow band phase sensitive detector (psd) operating at the dither frequency,

$$\epsilon_{psd} = (2CH_i \sin \omega_i t) H_s \qquad (2.5)$$

A trigonometric identity reveals that the quadratic term in (2.4) actually shows up at $2\omega_i$.

2.4 Optical Control Loop

The source of the optical control loop is the laser input. A thorough evaluation of laser sources is discussed in Appendix II. The prototype instrument uses a Uniphase 1103-605 He-Ne gas laser. This source was selected because its light is in the visible regime, which facilitates working with the interferometer, and its long coherence length eliminates the need to carefully match the interferometer path lengths.

The optical control loop has best sensitivity when locked in quadrature, where the relative phase of the light in the two legs is (2n+1) /2, n being an integer. The primary function of this loop is to maintain quadrature to provide a stable baseline for the magnetic detection circuitry.

Analysis of the interferometer response at the output of the difference amplifier gives

$$\Delta V = K_D(\theta_o + \theta_s) \qquad (2.6)$$

where ΔV = voltage at the difference amplifier,

K_D = optical gain from laser power, modulation depth, photodiode responsivity, and preamp gain,

θ_s = phase shift from magnetic and other induced signals,

θ_o = phase shift from fiber path and thermal mismatch.

The θ_o term varies much slower than the time scale of interest, and it can be treated as constant. Figure 2.4 shows a block diagram of the optical control loop.

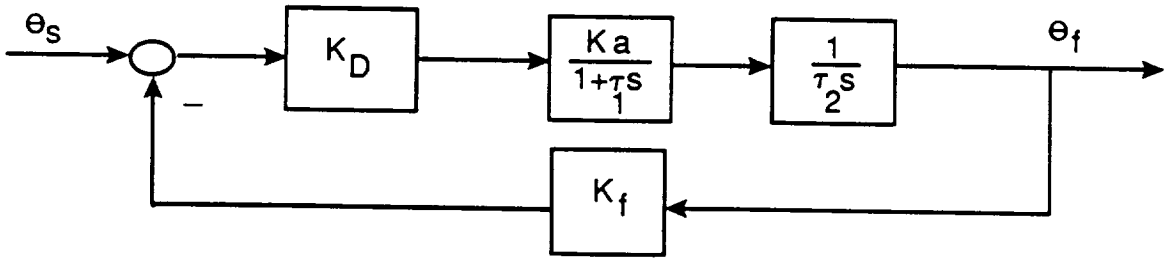

TDW92091

Figure 2.4 Optical Diagram of Optical Control Loop

The forward path of the loop can be represented by a second order transfer function

$$G_{OL}(S) = \frac{K_D K_a}{(1+\tau_1 s)(\tau_2 s)}, \qquad K_L = \frac{K_a}{(1+\tau_1 s)(\tau_2 s)} \tag{2.7}$$

where K_a = optical loop gain of the inverting amplifier
τ_1 = time constant of the low pass filter
τ_2 = time constant of the integrator.

The feedback path contains the pzt response

$$K_f(s) = \frac{K_o \omega_o^2}{\omega_o^2 + s^2 - \gamma s} \tag{2.8}$$

where K_o = low frequency pzt conversion gain
ω_o = pzt resonance frequency
γ = pzt damping ratio

Thus, the closed optical loop transfer function is given by,

$$G_{CL}(s) = \frac{\frac{K_D K_a}{\tau_1 \tau_2}}{s^2 + \frac{1}{\tau_1} s + \frac{K_D K_a K_f}{\tau_1 \tau_2}} \tag{2.9}$$

The measured pzt radian/volt conversion factor was K_f = 17.26 rad/V. The resonant frequency of the pzt was ω_o = 25 KHz.

From the system block diagram in Figure 2.4, the optical feedback phase shift $\theta_f(\omega)$ is given by

$$\theta_f(\omega) = K_D K_L (\theta_s - K_f \theta_f) = \left(\frac{K_D K_L}{1 + K_D K_L K_f} \right) \theta_s(\omega) \qquad (2.10)$$

For high gain, $K_D K_L K_f >> 1$, ideal lock occurs.

$$\theta_f(\omega) = \frac{1}{K_f} \theta_s(\omega) \qquad (2.11)$$

Typically, $K_D K_L K_f$ is on the order of 100 or greater.

2.5 Magnetic Loop

When the interferometer is locked in quadrature, the optical phase shift to the transducer response is given by

$$\theta_H = CkLH_a^2 \qquad (2.12)$$

where k = optical wavenumber
L = length of active fiber on the transducer

The low frequency signal can be extracted from (2.5) by a narrow band phase sensitive detector, thus, the terms in (2.4) at dc and $2\omega_i$ are rejected by the psd. Figure 2.5 shows a block diagram of the magnetic control loop.

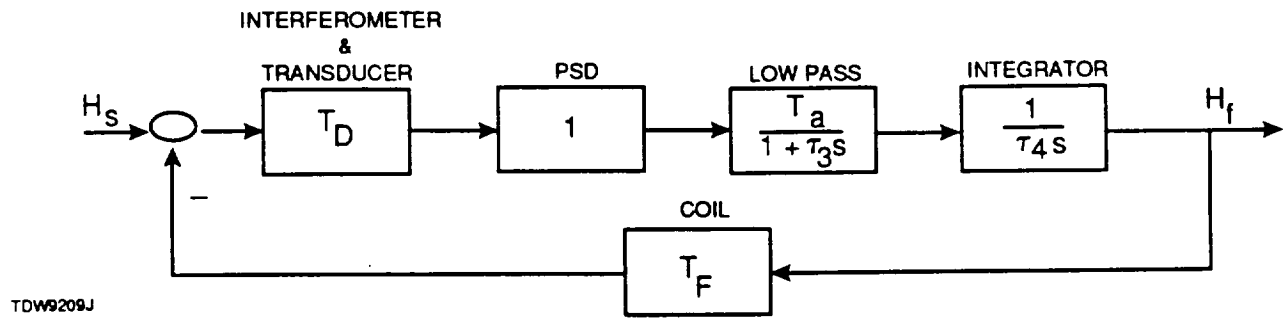

Figure 2.5 Block Diagram of the Magnetic Control Loop

The interferometer gain of the magnetic signal of is given by

$$T_D = 2CkLH_s \tag{2.13}$$

The reference signal of the psd is tuned in phase with the magnetically sensitive part of the interferometer response. The output of the psd is quite complex; however, as an approximation, the psd can be modelled as a block with unity gain.

A second order transfer function is used in the forward path,

$$T_{OL}(s) = \frac{T_D\, T_a}{(1 + \tau_3 s)(\tau_4 s)} \cdot \tag{2.14}$$

The feedback magnetic coil T_F was designed with the following gain.

$$T_F = 20\ \frac{\text{gauss}}{\text{amp}} \times .01\ \frac{\text{amp}}{\text{V}} \tag{2.15}$$

The closed loop transfer function is given by

$$T_{CL}(s) = \frac{\dfrac{T_D\, T_a}{\tau_3\, \tau_4}}{s^2 + \dfrac{1}{\tau_3}\, s + \dfrac{T_D\, T_a\, T_F}{\tau_3\, \tau_4}} \tag{2.16}$$

3.0 Electronic Hardware

The detection, control, and signal processing electronics have been reduced to printed circuit boards and inserted into their respective slots in a card cage. Each board is plugged into the FIG motherboard, which contains all the interconnections between cards. The individual electronic schematics are shown in Appendix III.

The electronics hardware consists of nine 4" x 6" boards which are listed below. Block diagrams have been drawn to provide a description of each circuit function.

- Spacemag Block Diagram
- Pre-Amp
- Optical Reset
- Magnetic Feedback Control
- Reference Generator
- Demagnetization Control
- Summing Amp
- Coil Driver
- I/O Control
- Anti-Aliasing Filter
- Motherboard

The block diagram of the overall system is also shown in Appendix III. The major system components include the power supply, laser source, optical feedback loop, magnetic feedback loop, interferometer, transducer, and controller/data acquisition system.

3.1 Optical Loop Circuits

3.1.1 Pre-Amp

The pre-amp board contains the mechanisms required to detect the interferometer light outputs, convert current to voltage, difference the signal, and amplify the difference signal, as shown in Figure 3.1.

The two light outputs are detected by PIN-040-A photodetectors mounted in Ofti connectors. The PIN-040-A has a responsivity of 0.3 mA/mW for 633 nm light. The current signals from the photodetectors are converted into voltage signals by the pre-amps with a gain equal to the sum of the feedback resistors in the pre amp circuit.

The two interferometer output signals are differenced by a unity gain difference amp. A variable resistor is used to adjust the gain of one pre-amp to match that of the other. The difference signal goes to a variable gain amplifier. All the components that perform these functions are located on a 4" x 4" board that is placed between the transducers in the sensor inside the sensor head compartment.

Four twisted, shielded pairs are connected to this board. Two power supply lines, +15 V and -15 V, and ground come from the battery. Also, the signal from the difference amp, containing the reference and gradient modulated signals, goes to the magnetic feedback control and gradient feedback control boards. The variable gain amp signal is connected to the optical reset circuit.

3.1.2 Optical Reset

The variable gain amp signal comes from the pre-amp circuit onto the optical reset circuit where it goes through a low pass filter and integrator, as shown in Figure 3.2. The optical control loop has a bandwidth of 3 KHz. The feedback voltage is buffered by a high-power op amp and connects to the pzt transducers.

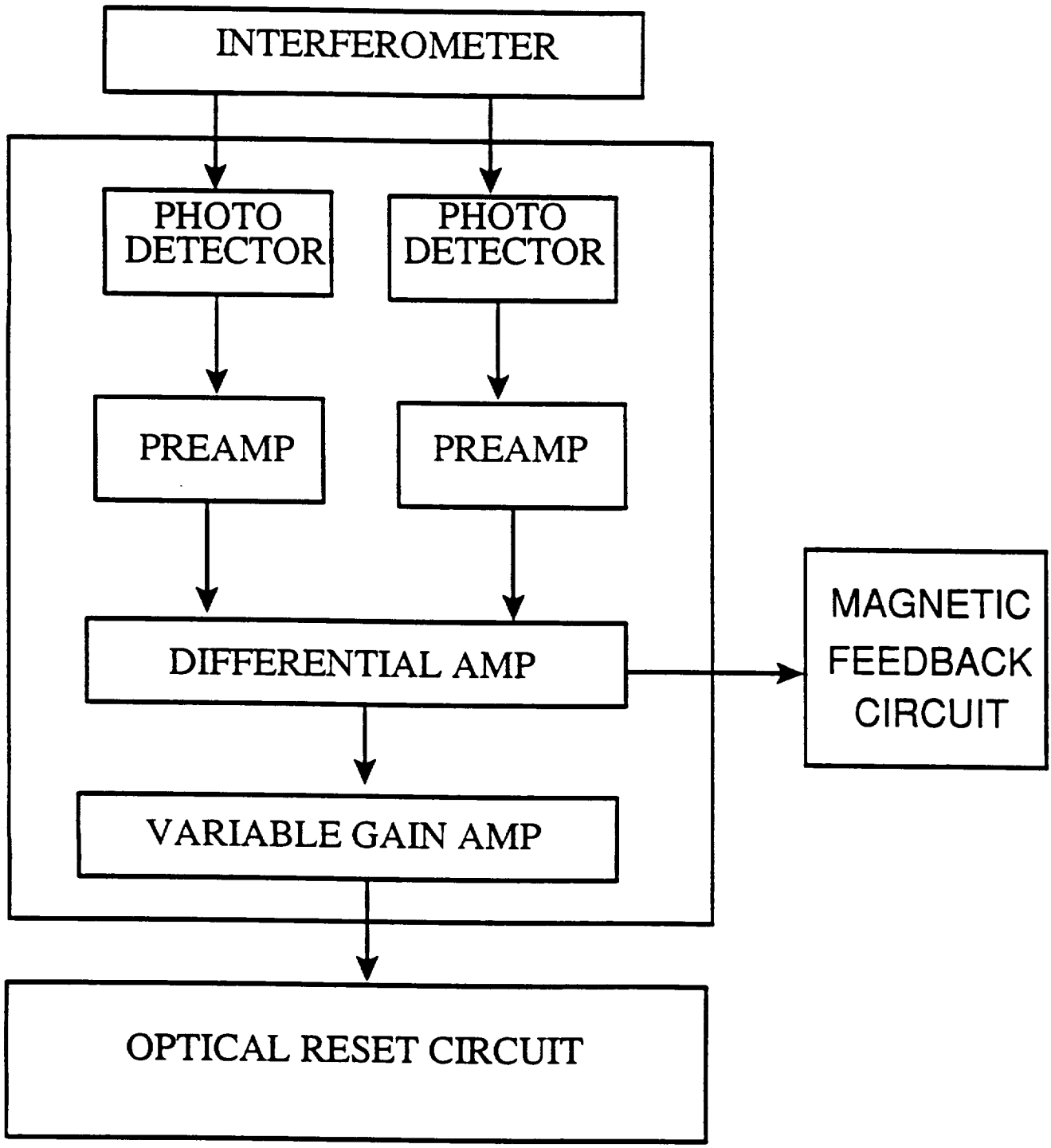

Figure 3.1 Pre-Amp Circuit Block Diagram

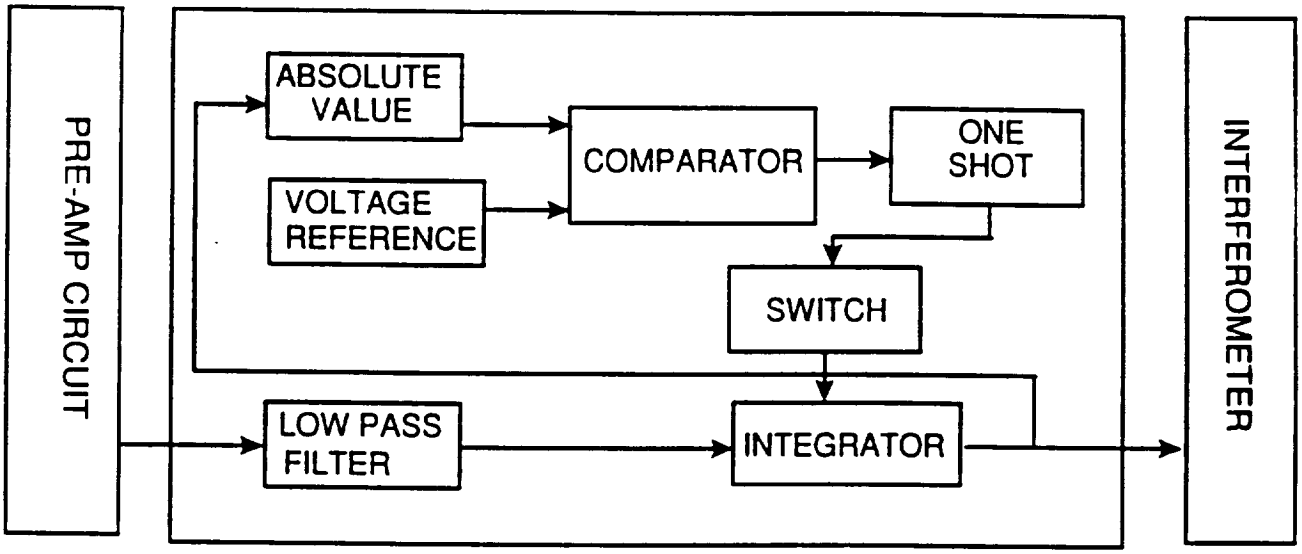

Figure 3.2 Optical Reset Circuit Block Diagram

Mechanical and environmental perturbations may cause the feedback signal to drift to either voltage rail. Thus, a reset feature is incorporated to prevent the integrator from saturation. The integrator output is passed through an absolute value circuit, and the output signal goes to a comparator. A reference voltage level is set at 12 V. Thus, when the integrator signal level reaches 12 V, the comparator triggers the one-shot, which closes a switch and resets the integrator.

Ideally, the optical control loop would be critically damped $\delta_o = .707$, with a natural cutoff frequency of about $\frac{\omega_{no}}{2\pi} = 300$ Hz. These parameters determine the time constants τ_1 and τ_2 from (2.9).

$$\frac{1}{\tau_1} = 2(.707)(300)(2\pi) = 2\delta_o\omega_{no} \tag{3.1}$$

$$\frac{K_D K_a K_f}{\tau_1 \tau_2} = \omega_{no}^2 \tag{3.2}$$

From the schematic, the following values are used.

$$\tau_1 = R_{10}C_3 \qquad \tau_2 = R_{11}C_4 \tag{3.3}$$

$$R_{10} = 375\ k\Omega$$
$$C_3 = 1\ nf$$
$$R_{11} = 375\ k\Omega$$
$$C_4 = 47\ nf$$

However, substantial laser noise appears, and the optical gain K_D varies with time. Thus, a 1 M potentiometer replaced R_{10} to allow the time constant τ_1 to be easily adjusted.

3.2 Magnetic Loop Electronics

3.2.1 Magnetic Feedback Control

The magnetic feedback control circuit, shown in Figure 3.3, performs the functions of the magnetic control loop. The output of the difference amp on the pre-amp circuit contains the modulated magnetic signal around 10 KHz. This signal passes through a 4-pole high pass filter with a cutoff frequency at 3 KHz. The filtered signal is demodulated by a phase sensitive detector, which is set to unity gain.

Similar to the optical control loop, the magnetic control loop is desired to have critically damping, $\delta_m = .707$, and a cutoff frequency of about $\frac{\omega_{nm}}{2\pi} = 300$ Hz. These parameters determine the time constant values in (2.17).

$$\frac{1}{\tau_3} = 2\delta_m \omega_{nm} \tag{3.4}$$

$$\frac{T_D\, T_a\, T_F}{\tau_3\, \tau_4} = \omega_{nm}^2 \tag{3.5}$$

From the schematic, the following values are used.

$$\tau_3 = R_9 C_6 \qquad \tau_4 = R_{10} C_7 \tag{3.6}$$

$$R_9 = 150\ k\Omega$$
$$C_6 = 0.1\ \mu f$$
$$R_{10} = 34\ k\Omega$$
$$C_7 = 1\ nf$$

The reference frequency to the psd is produced by the reference signal generator, which is the same as the dither frequency on the magnetic transducer. This reference frequency is phase shifted to be in phase with the most magnetically sensitive part of the modulated signal. This phase shifting must be done experimentally.

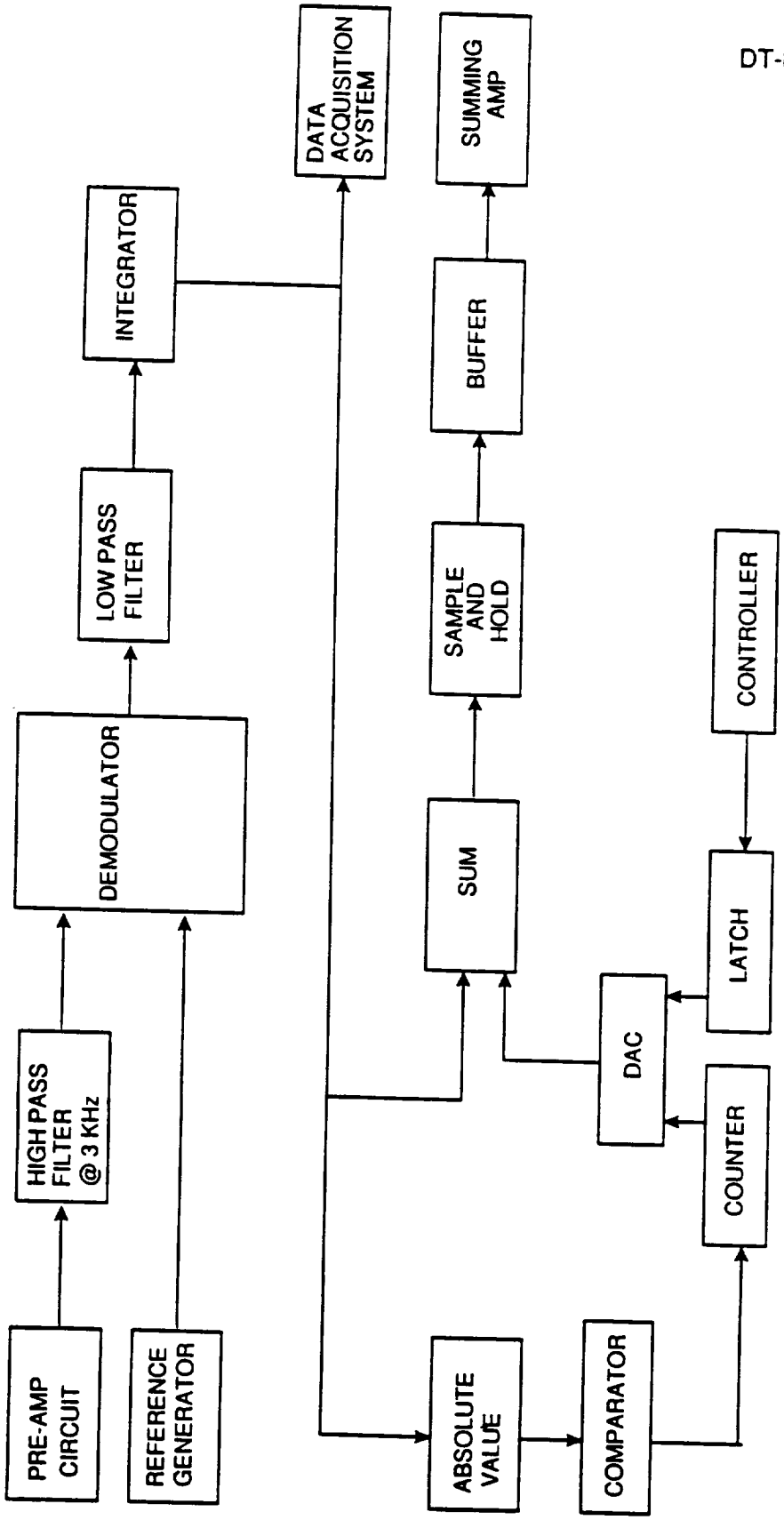

Figure 3.3 Magnetic Feedback Control Block Diagram

The demodulated signal passes through a low pass filter and integrator set to a cutoff frequency of 100 Hz. The output goes through a sequence of anti-aliasing filters, and is collected by the data acquisition system.

The magnetic feedback must be able to measure magnetic fields up to 10^5 gamma and detect fields as low as 0.01 gamma. In order to measure this dynamic range, the feedback circuit resets at every 10 V, and the computer controller keeps track of the total field value by the number of resets that have occurred.

A 16 bit DAC is used to generate the offset on the magnetic coil to null out residual magnetic fields on the transducer. The analog feedback signal is scaled to produce a magnetic field equivalent to the low byte of the DAC. Whenever the feedback reaches +10 V or -10 V, the integrator is reset, and the high byte of the DAC keeps track of the reset value.

The reset occurs either at +10 V or -10 V by passing the integrator output through an absolute value circuit, and firing a comparator at the proper voltage level. The comparator in turn activates a one-shot, which closes a switch and shorts out the capacitor on the integrator. At the same time, the comparator triggers a sample and hold to maintain the feedback signal at the correct value long enough for the high byte of the DAC to change by 1 LSB.

In this fashion, up to $2x10^5$ gamma may be measured by summing the magnetic field tracked by the high byte of the DAC with the analog output of the feedback circuit. At the same time, the magnetic feedback circuit can measure fields at a calibrated factor of 6.44 mV/gamma.

3.2.2 Reference Generator

The reference generator, shown in Figure 3.4, produces the dither signal to modulate the magnetic transducer and the reference signal for the psd. The dither signal is produced by a signal generate chip which is able to generator frequencies between 1 KHz and 12 KHz. In characterizing the transducer, the dither frequency is varied throughout its range to determine the frequency where the transducer has the greatest sensitivity. The quality of the generated sine wave can be tuned with two distortion pots. A non-inverting amplifier is used to adjust the dither amplitude.

$$H_{\omega_i}(t) = H_i \sin\omega_i t \quad i = x, y, z \tag{3.7}$$

where H_i is the amplitude of the dither
and a reference signal for the phase sensitive detector,

$$H_{\omega_i}(t) = H_i \sin(\omega_i t + \delta_i) \quad i = x, y, z \tag{3.8}$$

where δ_i is an arbitrary phase.

The magnitude of the carrier signal is adjustable up to 2 gauss, but is usually operated around 0.2 gauss.

The reference generator also produces the reference signal for the demodulator. A phase shifter is used to adjust the reference signal in phase with the magnetically sensitive portion of the difference waveform. Also, a non-inverting amp adjusts the magnitude of the reference signal. The input signal is ac coupled to produce a symmetric waveform about ground.

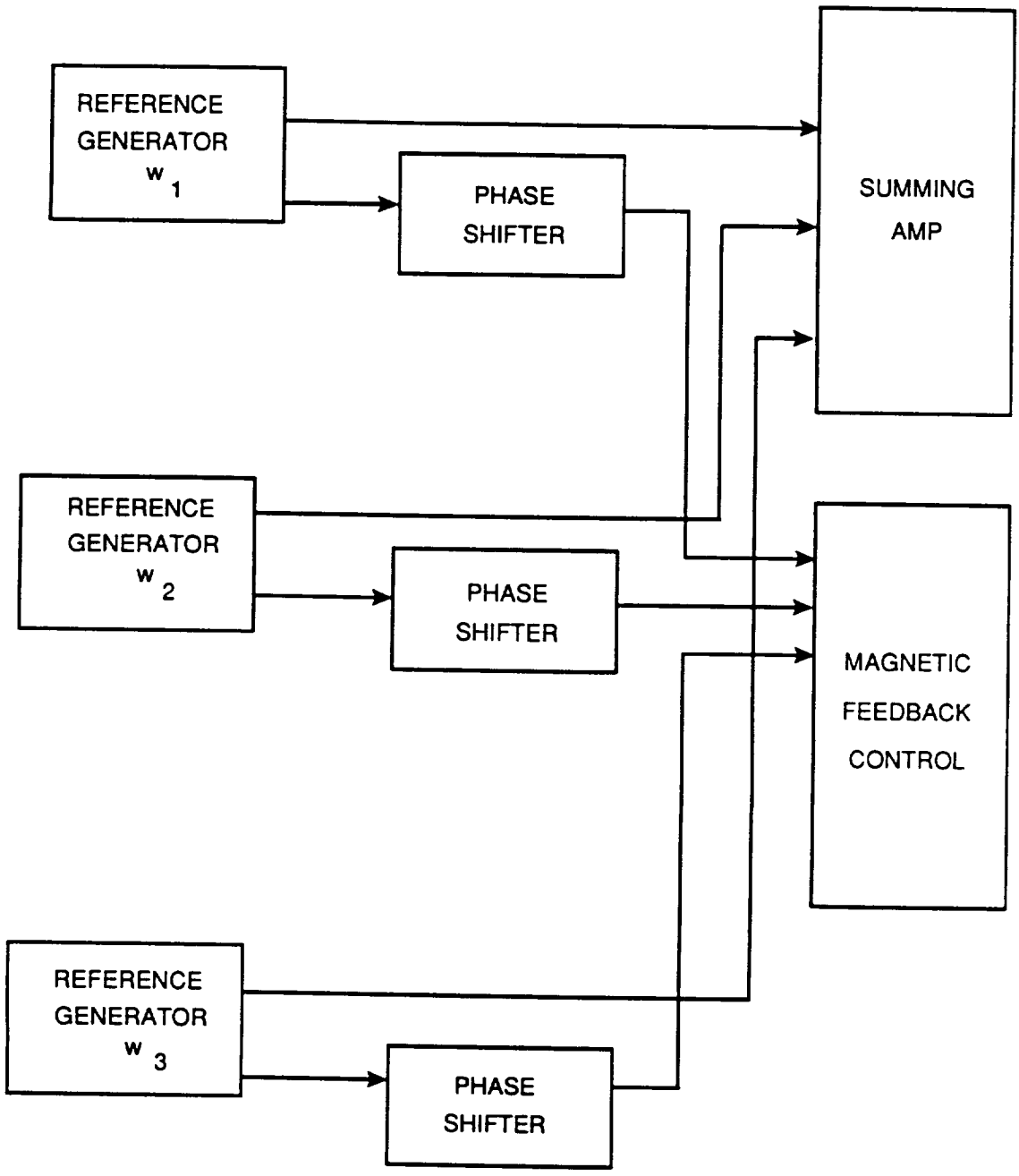

Figure 3.4 Reference Generator Block Diagram

3.2.3 Demagnetization Control

The demagnetization control circuit, shown in Figure 3.5, applies a linearly increasing sinusoidal magnetic field up to a peak value and then a linearly decreasing sinusoidal field to the metallic glass transducers. The transducers must be demagnetized to remove magnetic offsets and other preferred magnetic orientations. Demagnetization ensures maximum sensitivity, dynamic range, and repeatable measurements. Applying a sinusoidal signal of decreasing amplitude to the transducer effectively drives the metallic glass through numerous hysteresis loops of diminishing size, converging to a minimum offset value. Each transducer is usually demagnetized three times each with peak values of 2 gauss, 1 gauss, and 0.4 gauss. The three transducers are then demagnetized simultaneously at a peak value of 0.2 gauss before all of the channels are locked.

The demagnetization process is initiated by the computer controller. A switch becomes activated which allows an integrator to ramp up to its peak value. This linearly increasing signal is multiplied by a 100 Hz sine wave, and it is on for 10 seconds. At that point, the switch shuts off the increasing signal and requires the integrator to ramp down to zero. This downward cycle takes 20 seconds. The magnitude of the output signal is determined by a gain control device, which can be set for discrete gain values.

3.2.4 Summing Amp/Coil Driver

Each metallic glass transducer is driven by several magnetic fields produced by the magnetic feedback coils. The input signals from various sources are applied through the summing amp and the current is provided by the high power coil driver circuits, shown in Figure 3.6. Each magnetic field coil sees three fields, the dither, demag, and magnetic nulling fields. The dither fields are created by the reference generator, discussed in section 3.3. The demag fields can be applied to each transducer separately or individually.

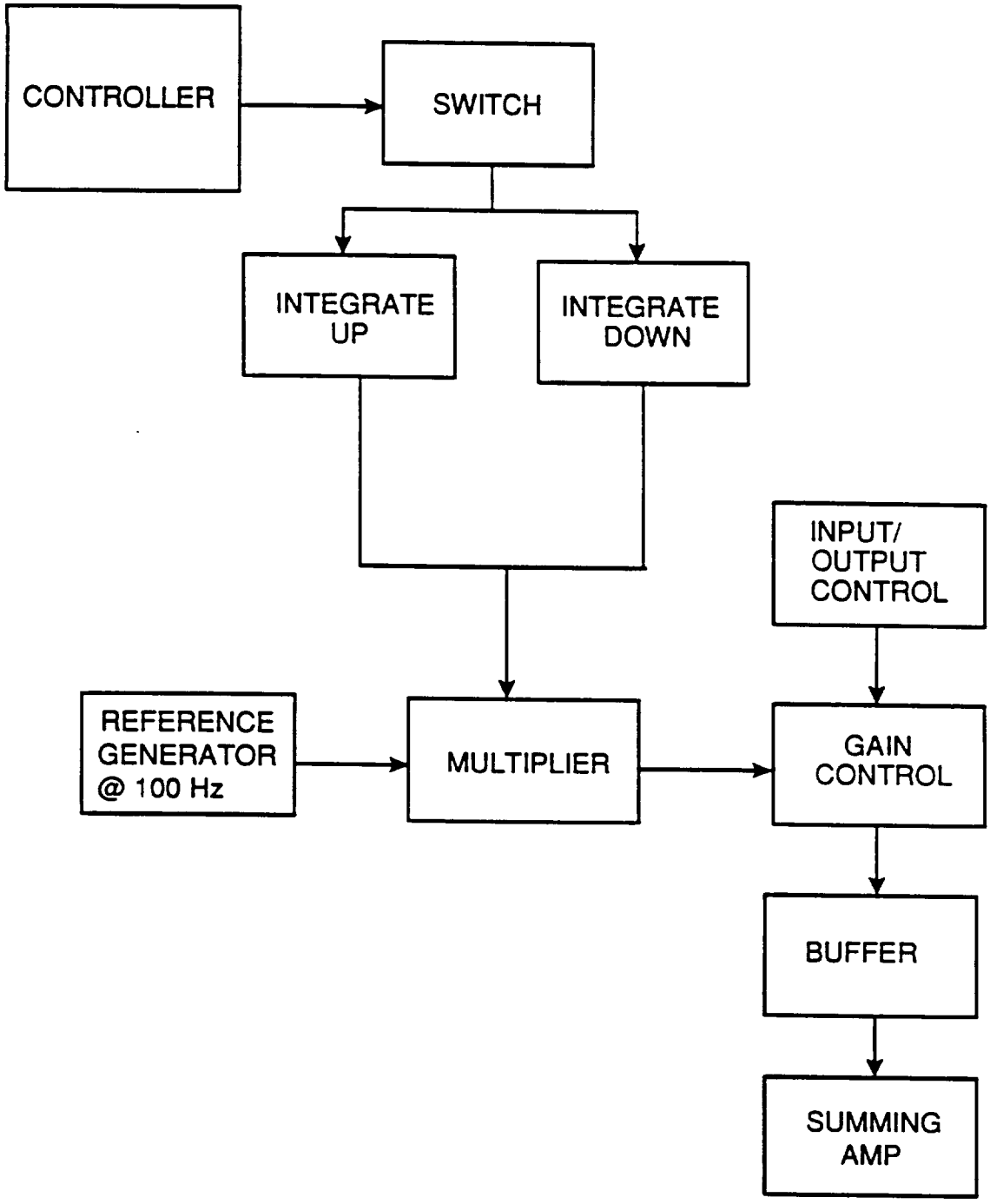

Figure 3.5 Demagnetization Control Block Diagram

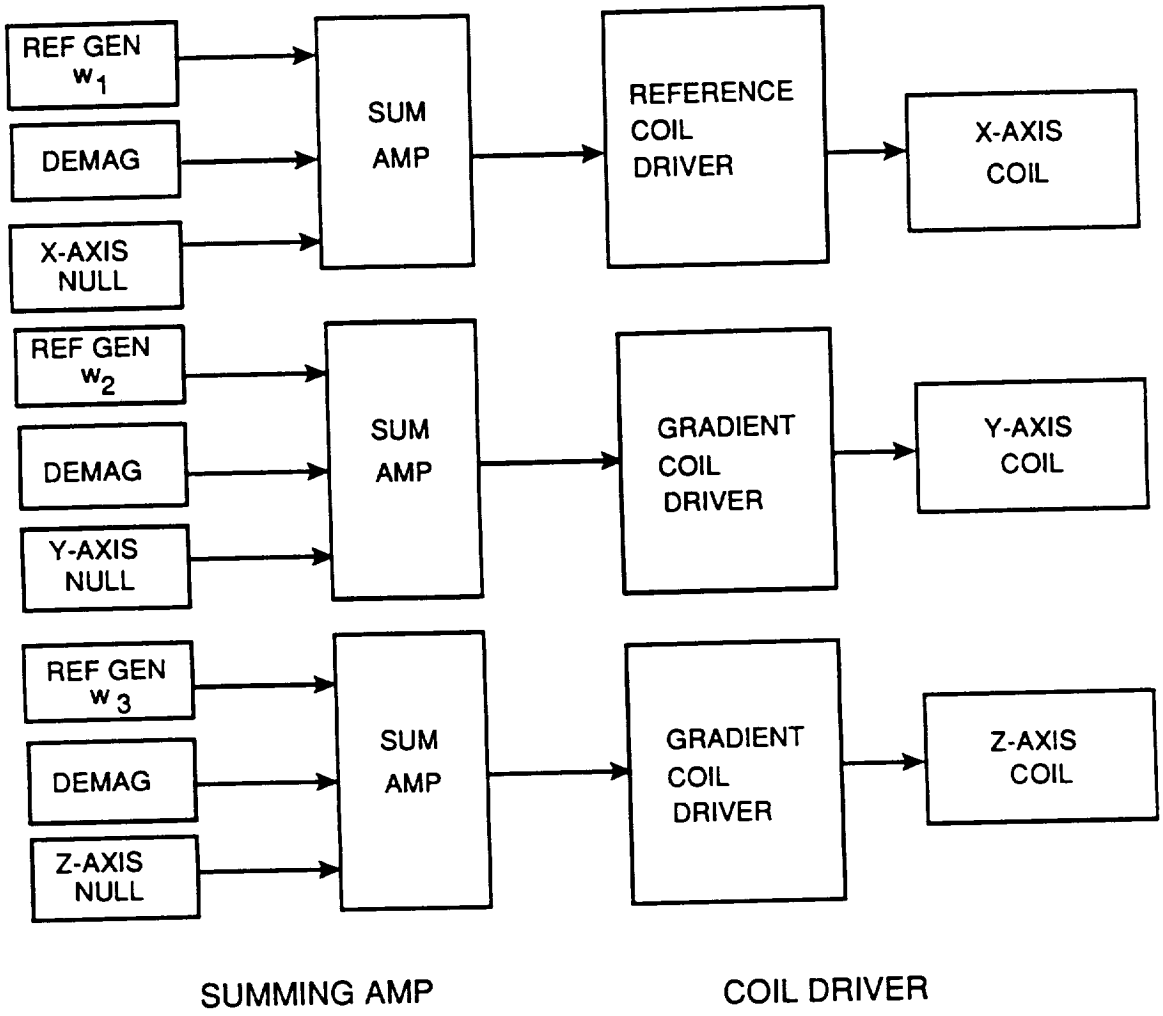

Figure 3.6 Summing Amp and Coil Driver Block Diagram

The coil driver amplifer in each channel drives the coil with the sum of all three signals. This amp is capable of providing up to 5 A of current. The power amplifier is arranged in a feedback configuration to minimize drift. The magnetic field coils are driven in series with a precision 100 ohm resister to provide a means to measure the drive signal.

3.3 Control Circuits

3.3.1 Input/Output Control

The input/output control card, shown in Figure 3.7, is the means by which the computer controller activates the commands for operation using a 6 bit address bus and an 8 bit data bus. The I/O control function is used setting up the DACs on the magnetic feedback control circuits, running the demagnetization procedure, locking the magnetic control loop, and collecting the data.

When the magnetometer instrument is set up, the residual magnetic field on each transducer must be nulled in the open loop condition. This task is accomplished by establishing a nulling field on the transducer coil by setting the high and low bytes of the DAC. Thus, the nulling field can be applied with 16 bit accuracy.

Once the ambient field has been nulled, the I/O control card selects a transducer to be demagnetized, using the start demag function. If a residual signal appears, which is usually the case, the demag procedure is repeated. The load high byte and load low byte commands once again zero the offset and the transducer demagnetization is repeated at a lower demag gain factor. This process is repeated until less than 0.1 gamma offset is observed after demag.

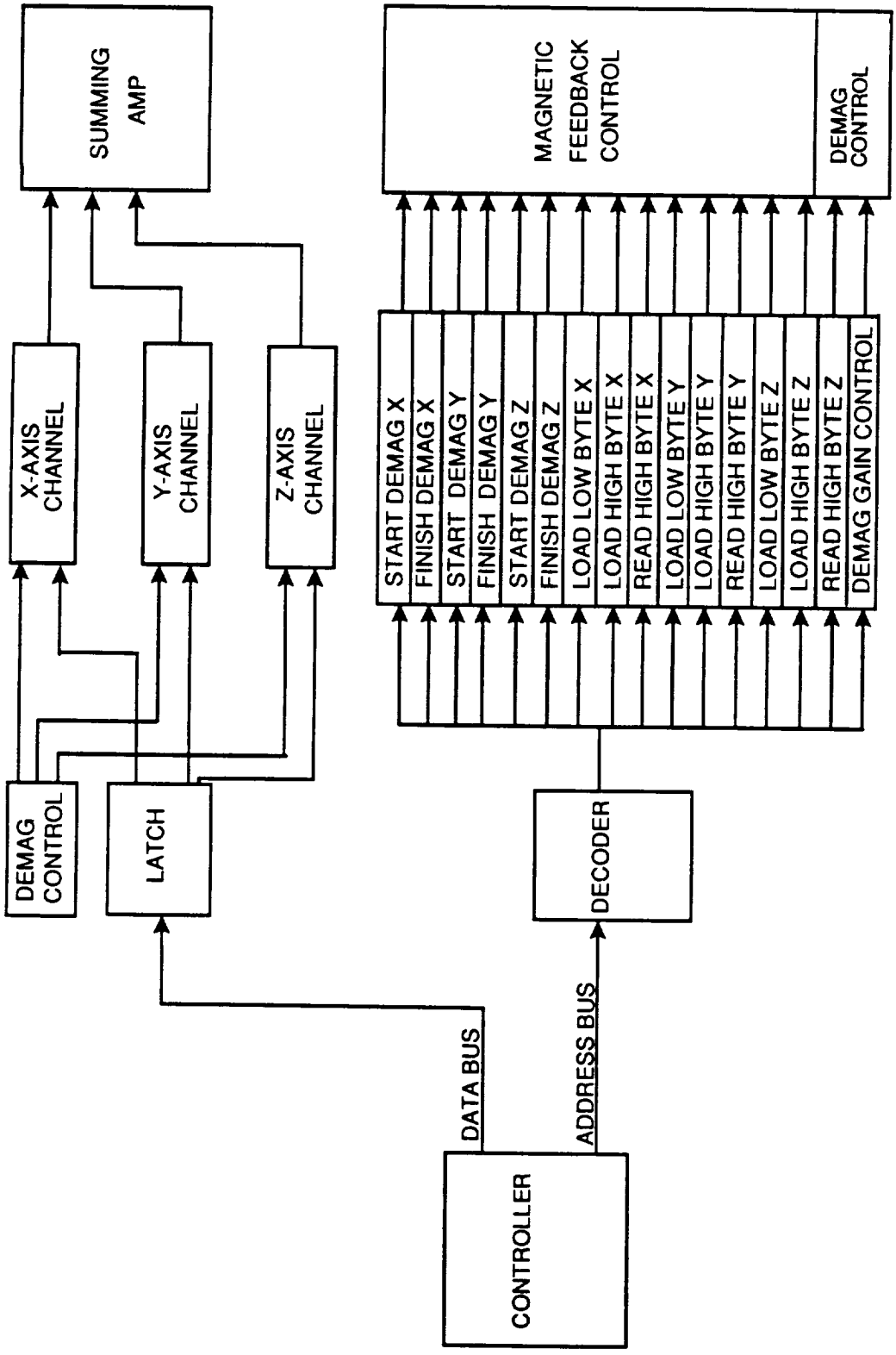

Figure 3.7 Input/Output Control Block Diagram

The magnetic feedback control loops are locked when the I/O control activates the finish demag command. The I/O control monitors the high byte on each DAC during the data acquisition process using the read high byte command. The high byte data is added to the analog output value from the magnetic feedback control circuit to give the total field or gradient value. Each channel can be locked separately.

3.3.2 Anti-Aliasing Filter

The analog output of the magnetic feedback control circuit is passed through a series of anti-aliasing filters shown in Figure 3.8. This section consists of four identical two pole Butterworth low pass filter with a cutoff frequency of 15 Hz. The magnetic and gradient fields of interest are 1 Hz and below; however, the filters are set at a 15 Hz cutoff to collect data which allows for motion by the instrument operator.

3.3.3 Motherboard

The system motherboard is shown in Appendix III. This board contains the connectors that attach to each card. All the jumpers between cards, power supply traces, and signal lines are routed on this board between the cards.

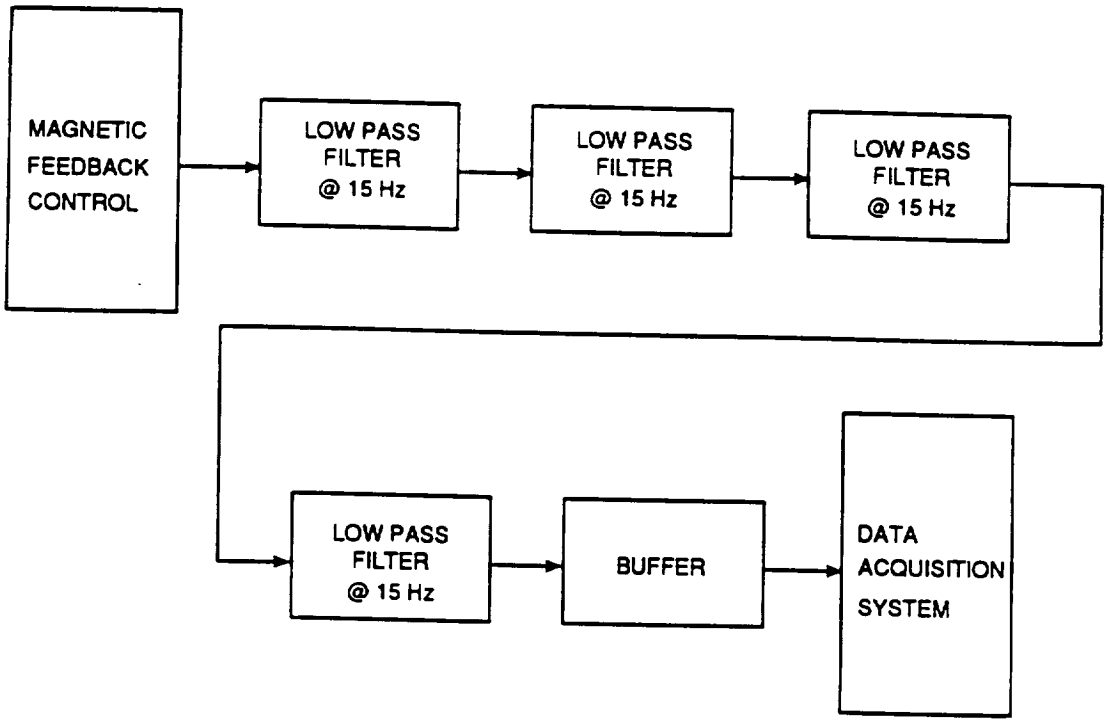

Figure 3.8 Anti-Aliasing Filter Block Diagram

4.0 COMPUTER HADWARE AND SOFTWARE

4.1 Computer Hardware

The computer being used for the data acquisition and control of the Spacemag instrument is a Dell 286 laptop computer. It has a 80286 processor running at 8 MHz with 2 Mb of RAM. It is also running a 80287 floating-point math co-processor. It has a hard disk drive with 40 Mb storage capacity, and a 5.25 inch floppy disk drive with 1.2 Mb storage capacity. It is running the IBM-OS/2 1.0 operating system.

Control of the Spacemag instrument is done through a parallel digital input/output interface from MetraByte Corporation (Model PIO12). It has three input/output ports, each eight bits wide. One port is used as an address port, one as a data port, and one as a control port. All these ports are connected to the computer interface board of the Spacemag instrument.

For the data acquisition, a Data Translation board, model DT2805/5716 is being used. It is an analog and digital input/output board with DMA (Direct Memory Access) capabilities. It has eight channels of analog input each with 16 bits of resolution. None of the digital input/output capabilities of this board are being used because the board cannot perform analog-to-digital conversion and digital input/output simultaneously. This is the reason the PIO12 board is being used.

4.2 Computer Software Description

The software can be functionally broken up into three procedures, as shown in Figure 4.1, where each procedure is performed by running a different program. These three procedures are: 1) Demagnetization of the Spacemag instrument (DEMAG); 2) Acquisition of data from the Spacemag instrument; and 3) Display of the

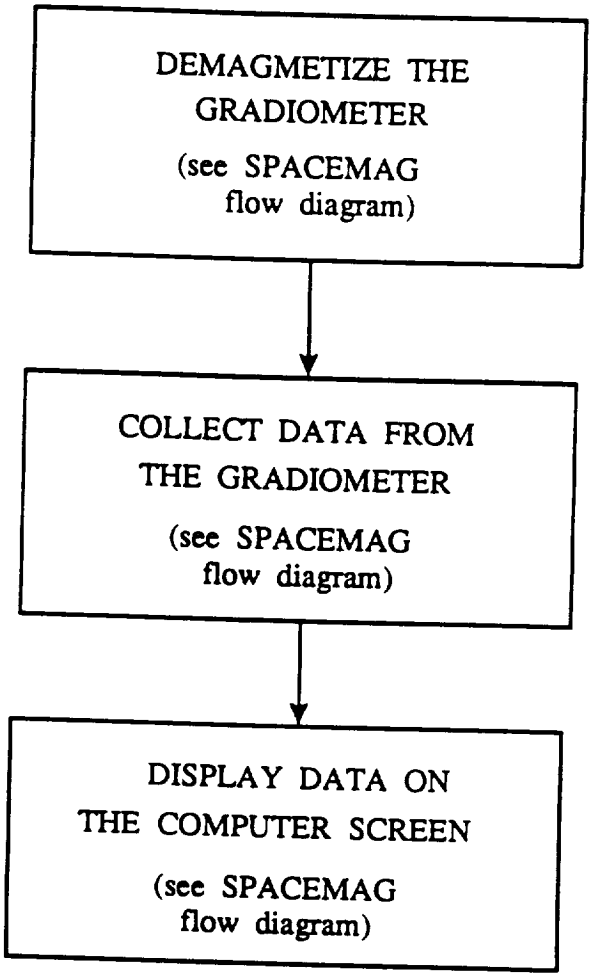

Figure 4.1 Spacemag Software Flow Diagram

acquired data on the computer screen. In order to drive the PIO12 board and the DT2805/5716 board, a single device driver was written to drive both of them. This device driver is called from the first two programs but the third one does not call it. The language used for the first two of these programs was Microsoft-C. The third program was written in Microsoft-Fortran. The device driver was written in assembly language for the 80286 and assembled using the Microsoft Macro Assembler. The following is a more detailed description of these programs.

4.2.1 Device Drivers

The source code for the device driver written to drive both the PIO12 board and the DT2805/5716 board is contained in the file DT2805.ASM. This device driver is callable from C programs through the OS/2 operating system. There are two main parts of the driver, one being the DT2805/5716 driver and the other being the PIO12 driver.

The DT2805/5716 device driver is broken up into four functions. These four functions are 1) Load the DT2805/5716 board with initial parameters; 2) Start the analog-to-digital conversion and DMA transfer; 3) Stop the analog-to-digital conversion and DMA transfer; and 4) Set the driver to do block transfers of a specified size.

Loading the initial parameters is done first. These parameters include gain, number of channels, sampling frequency, etc. The C code passes into the driver a structure filled with the values for these parameters. The driver then loads these parameters into the DT2805/5716 board one at a time.

To start the analog-to-digital conversion and DMA transfer, the C code makes a call to the device driver specifying this function and the driver sends the signal to the

DT2805/5716 board. The DT2805/5716 board is programmed to fill a circular DMA buffer in RAM on the PC with the data it acquires from the Spacemag instrument. The device driver keeps track of the memory being filled. When the C code wants data, it must request a block from the device driver. When a block of data has been filled by the DT2805/5716 board, the driver sends this block to the C code, along with the size of the block. The C code then processes this data and when it is finished processing, it request another block of data from the device driver. This continues until the C code needs no more data and makes a function call to stop the analog-to-digital conversion.

To stop the analog-to-digital conversion and DMA transfer, the C code makes a call to the device driver specifying this function and the driver sends the signal to the DT2805/5716 board. The board discontinues its acquisition and transfer of data.

The last function of this category controls the minimum size of the blocks of data that the device driver returns to the C code. When the driver is called, it does not return until it can fill a buffer of at least the size specified. This function also allows the driver to be programmed for no block transfer. This means that the driver does not wait for a certain number of bytes of data to be filled in the buffer. Instead, the driver returns immediately after it is called, returning the number of bytes it transferred. This allows the C code to be able to do large block transfers for data acquisition, or do small or no block transfers for monitoring of signals (fast response).

The PIO12 device driver is broken up into three functions. These three functions are 1) Initialize the board; 2) Read a data byte from the data bus; and 3) Write a data byte to the data bus. When the initialization of the PIO12 board is done, the three ports of the board are set as follows. Port A is setup as a bi-directional port and is connected

to the data bus of the interface board. Port B is setup as a strobed output port and is connected to the address bus of the interface board. Port C is setup as a control port and has some lines connected to control lines on the interface board and other lines connected to the strobe lines of ports A and B.

When the device driver receives a read call from the C code, it executes a read from the PIO12 board using the three ports. The driver first takes the address that is passed to it by the C code and sends it out onto the address bus through port A. This enables the data onto the data bus of the interface board. The driver then reads the data from the data bus through port B and returns this data to the C code. The appropriate handshaking lines are strobed through port C in order to do the above function.

A write is done in the same fashion. This time a data byte is put on the data bus through port A. After a settling time, the address is sent out through port B, which latches the data into registers on the interface board. This function is also used to send signals to the interface board without writing data. The device driver checks for certain addresses which correspond to these signals. If it gets one of these addresses, it skips the placement of data on the data bus and just sends the address which gets decoded into a signal on the interface board.

4.2.2 Demagnetization

The demagnetization of the Spacemag instrument is done by running a program called DEMAGSAC, whose software flow diagram is shown in Figure 4.2. This is an interactive, menu-driven program which interprets commands input from the keyboard of the computer and sends them to the Spacemag instrument via the PIO12 and the Spacemag interface board. This program makes calls to the PIO12 device driver to

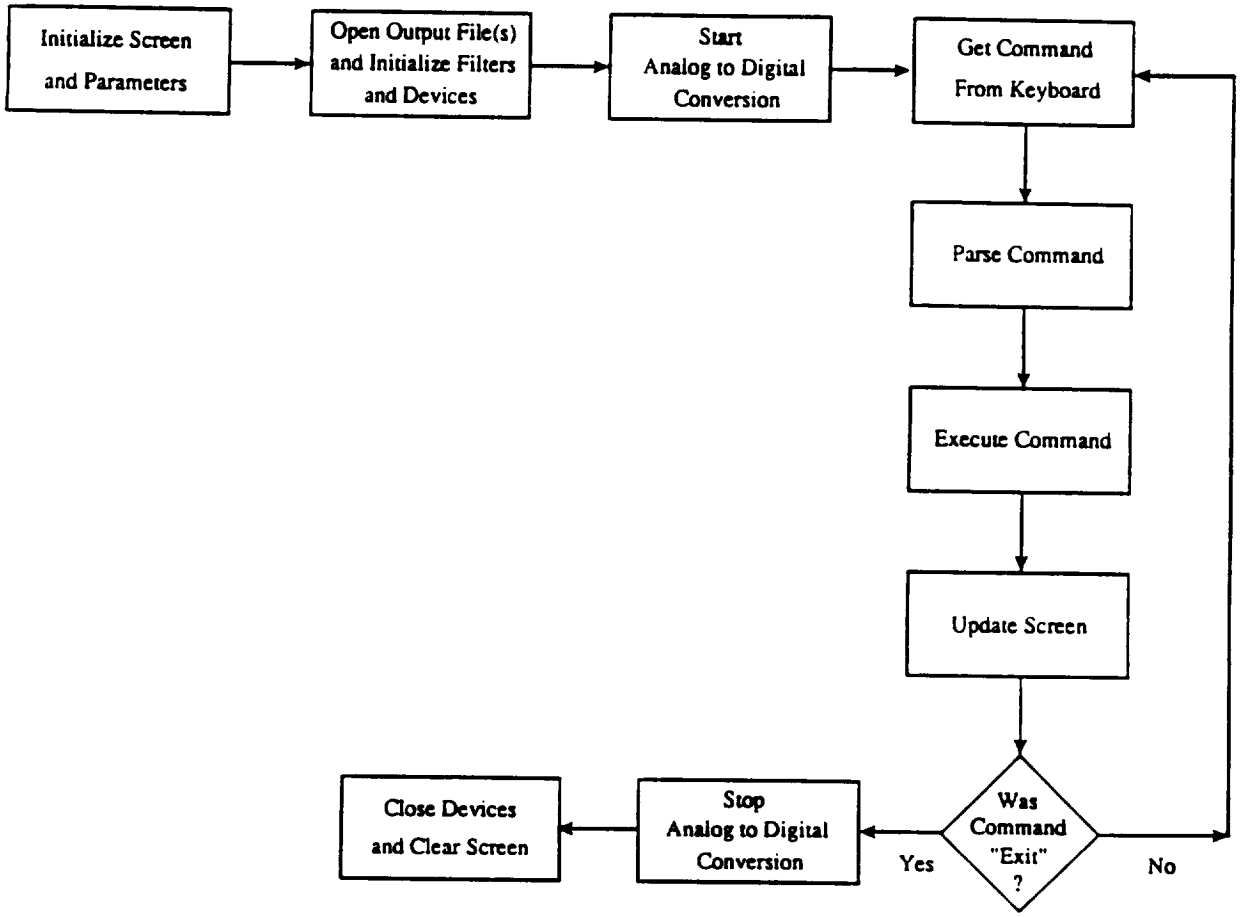

Figure 4.2 Demag Software Flow Diagram

transfer values and signals to and from the interface board. While waiting for commands to be entered, the status of some system parameters are displayed. These parameters include the value of the current offsets held in the digital-to-analog converters (DACs) and the value of the current demodulation output from the Spacemag instrument. Included in the set of commands are commands to adjust the offsets held in the DACs, set the dither channels, send a "demag" signal to the Spacemag instrument, adjust the gain of the "demag" signal, and lock the loops on specified channels.

When the program is started, the main menu and command prompt are displayed on the screen. Then some initialization of global parameters is done. Next, the program opens the device driver for the PIO12 and DT2805/5716 boards, and initializes both boards. Then the analog-to-digital conversion is started on the DT2805/5716 board. This is done with no block transfer so the screen can be updated quickly. The program now enters the main loop. This consists of getting a command from the keyboard, parsing the command, executing the command, and updating the screen. This is done until an "exit" command is received. When an "exit" command is received, the analog-to-digital conversion is stopped on the DT2805/5716 board, the device driver is closed, and the screen is cleared. Once the Spacemag instrument is demagnetized, the user can exit the program and go on to the acquisition of data.

4.2.3 Data Acquisition

The acquisition of data from the Spacemag instrument is done by running a program called GETDATA (this command actually calls "adcfltss", which is the code that is listed). The software flow diagram for the data acquisition is shown in Figure 4.3. This program prompts the user for some acquisition parameters such as the number of channels to sample, sampling frequency, length of run, filter cutoff, and decimation value. Once these values are entered, the program opens the device

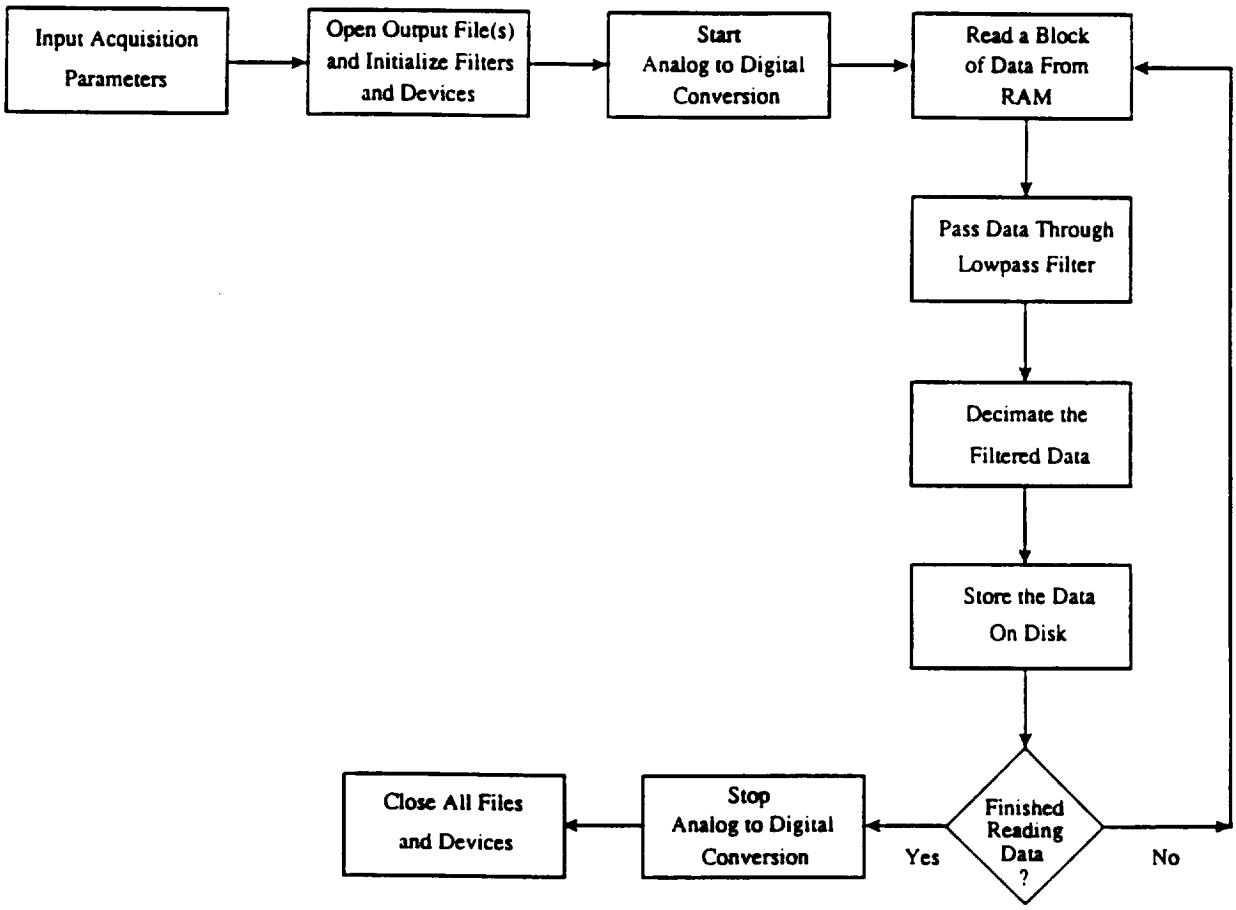

Figure 4.3 DAS Software Flow Diagram

driver for the PIO12 and DT2805/5716 boards, and initializes both boards. Then the analog-to-digital conversion is started on the DT2805/5716 board. This is done with block transfer to speed the acquisition. The program now enters the main loop. This consists of calling the device driver for the DT2805/5716 board to get a block of data. When the C code receives this block of data, it passes the data through a digital filter. The filter is a 4-pole Butterworth lowpass tangent filter. The filtered data is then decimated and stored in disk files. Each time this program is run, a new set of data files is created, one for each channel, so the data can be analyzed later. When enough datahas been collected, as told by the length of run, the signal to stop the analog-to-digital conversion is sent to the DT2805/5716 board. Then the device driver and all data files are closed and the program ends. Now the data must be displayed.

Data Display

The program that does the displaying of data on the computer screen is called GRFRUN. The display software flow diagram is shown in Figure 4.4. This program will prompt the user for the number of the run to be displayed. It then reads in the raw data from the files that were created using GETDATA (see above). This is done by constructing the filenames of each data file from the input run number. It reads from each file a two byte integer. The integer is then converted to a four byte floating point voltage. The reading and converting is done until the end-of-file is reached. Then the data is passed to a plotting package called PCGRAPH which plots the voltages vs. time on the computer screen. If desired, the graphs shown on the screen can then be plotted to a printer file for later plotting or the program can simply be exited. A helpful program exists called SHOWDATA. This program calls GRFRUN with the run number of the last run taken. It is useful for taking a run of data using GETDATA and then taking a quick look at it using SHOWDATA.

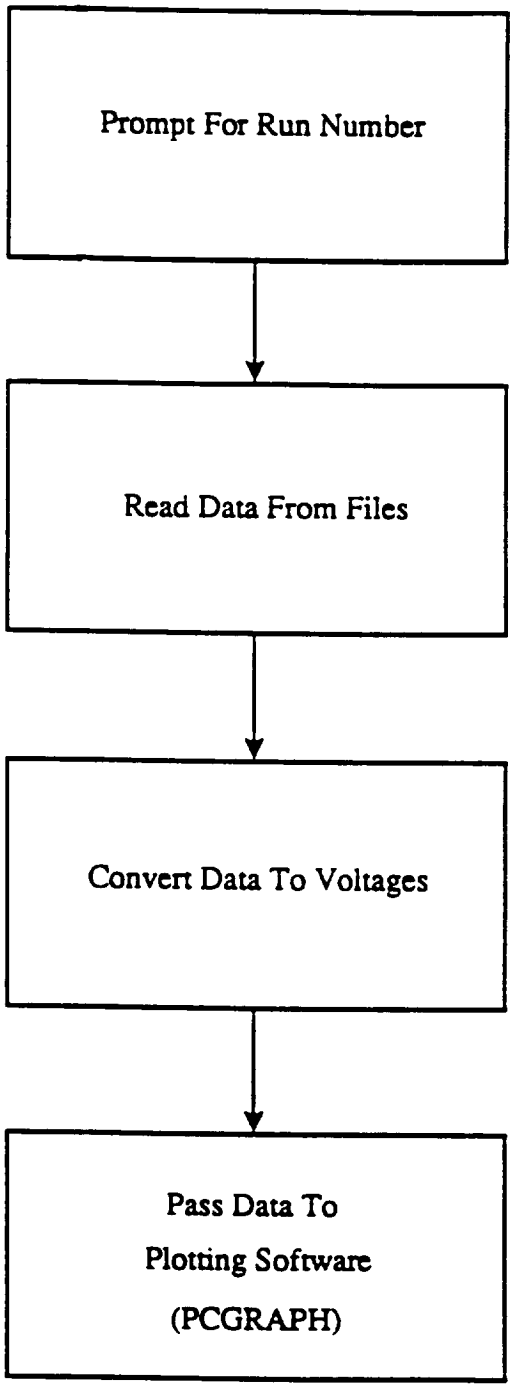

Figure 4.4 Display Software Flow Diagram

5.0 SPACEMAG ASSEMBLY

The Spacemag 3-axis magnetometer assembly consists of two interferometers with three magnetic field transducers in the x, y, and z directions. Also included in the interferometers are the pzt feedback elements, polarization controllers, bidirectional couplers, and laser source. The complete lab set-up is shown in Figure 5.1 with electronics, computer, and electronic and laser power supplies.

Each transducer is mounted on a 4 7/8" x 9 1/2" lexan block of thickness 1/2". The transducers are separated from each by 1/2" with a tolerance of less than 0.005 radians. The transducer mount is shown in Figure 5.2. In Figure 5.3, the pzt elements are shown. Each interferometer uses two pzts in parallel in the feedback loop, while a third is used to apply a test signal.

The magnetic field sensing element consists of fiber bonded onto a layer of metallic glass.

A 5" x 1" metglas strip is attached onto a plexiglas mandrel, shown in Figure 5.4, by a thin layer of oil. Single mode fiber is wrapped around the mandrel for 88 turns, and the fiber is glued down to the metglas strip near each end at a distance of 3.75" apart. The total active length of fiber is 330". The fiber pigtails leave this assembly wrapped around the cylindrical turning post.

The transducer housing is then placed into the magnetic coil form, shown in Figure 5.5. The number of coil form windings and coil design considerations are discussed in Appendix I. The primary considerations are to provide a homogeneous and uniform magnetic field given size limitations and interaction effects between sensors. The metglas, mandrel, fiber, and coil form are placed together into a transducer holder.

Figure 5.1 Complete Spacemag 3-axis magnetometer assembly is shown with signal processing electronics and data acquisition computer.

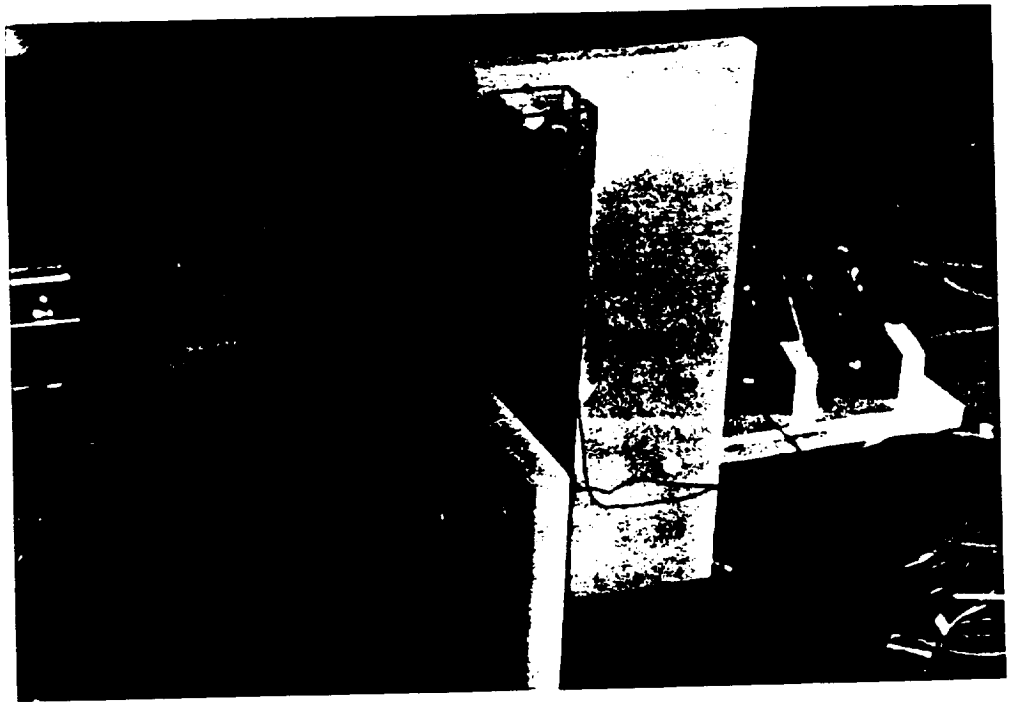

Figure 5.2 The three transducers are mounted as shown with 0.5" separation between axes.

Figure 5.3 Two pzt elements are used in the feedback loop for each interferometer, while another is used to apply a test signal.

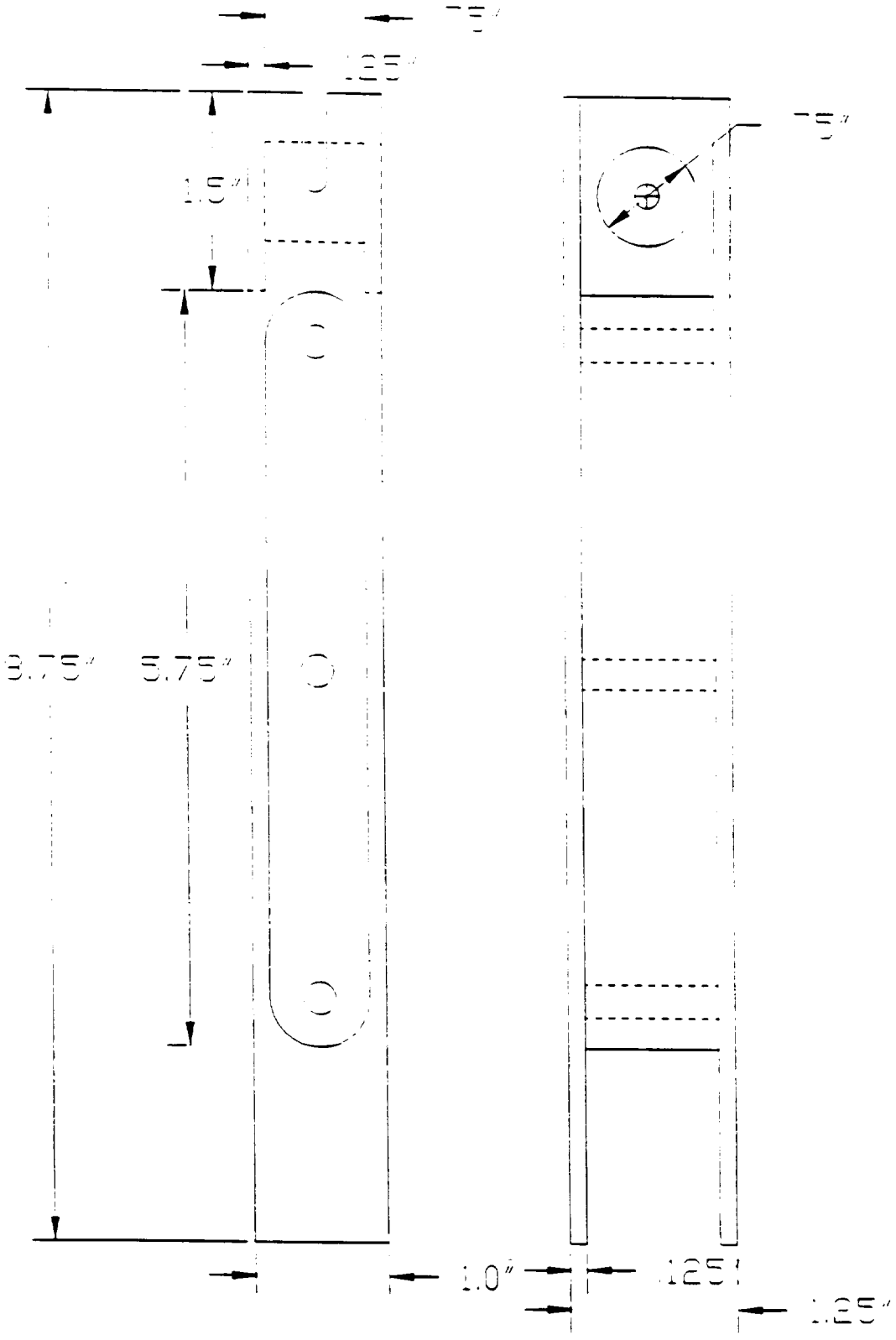

Figure 5.4 Transducer mandrel; Front and Side Views

The Uniphase laser, model number 1103-605, and dc power supply were contained in an 18" section of an acrylic tube. The laser tube was wrapped with fiberglass insulation to maintain a uniform temperture. Both ends of the acrylic tube was covered by plastic endpieces to protect the laser from air currents. The tube had a provision for a screwdriver to be inserted, which enables the coupler to be easily adjusted to optimize laser power. The laser output was connected to the fiber interferometer using a 3' pigtail.

A Dolch P.A.C. laptop computer was used in the data acquisition, digital processing, and data display of the three-axis magnetometer results. This unit is shown in Figure 5.6. The data acquisition was done using three A/D converters channels on a Data Translation board each with 16 bits of resolution. The details of operation are discussed in Section 4.0.

A major noise source comes from polarization fade between the light in the reference and transducer legs. This effect is discussed further in Section 8.3. The interference fringe visibility can be maximized by adjusting the polarization state of light in one leg relative to the other. This procedure is accomplished by rotating the polarization controller shown in Figure 5.7.

The optical detection, feedback control loops, and filtering functions of the system are done by a set of analog electronics shown in Figure 5.8. The circuit schematics are shown in Appendix III, while the functional descriptions are discussed in Section 2.0.

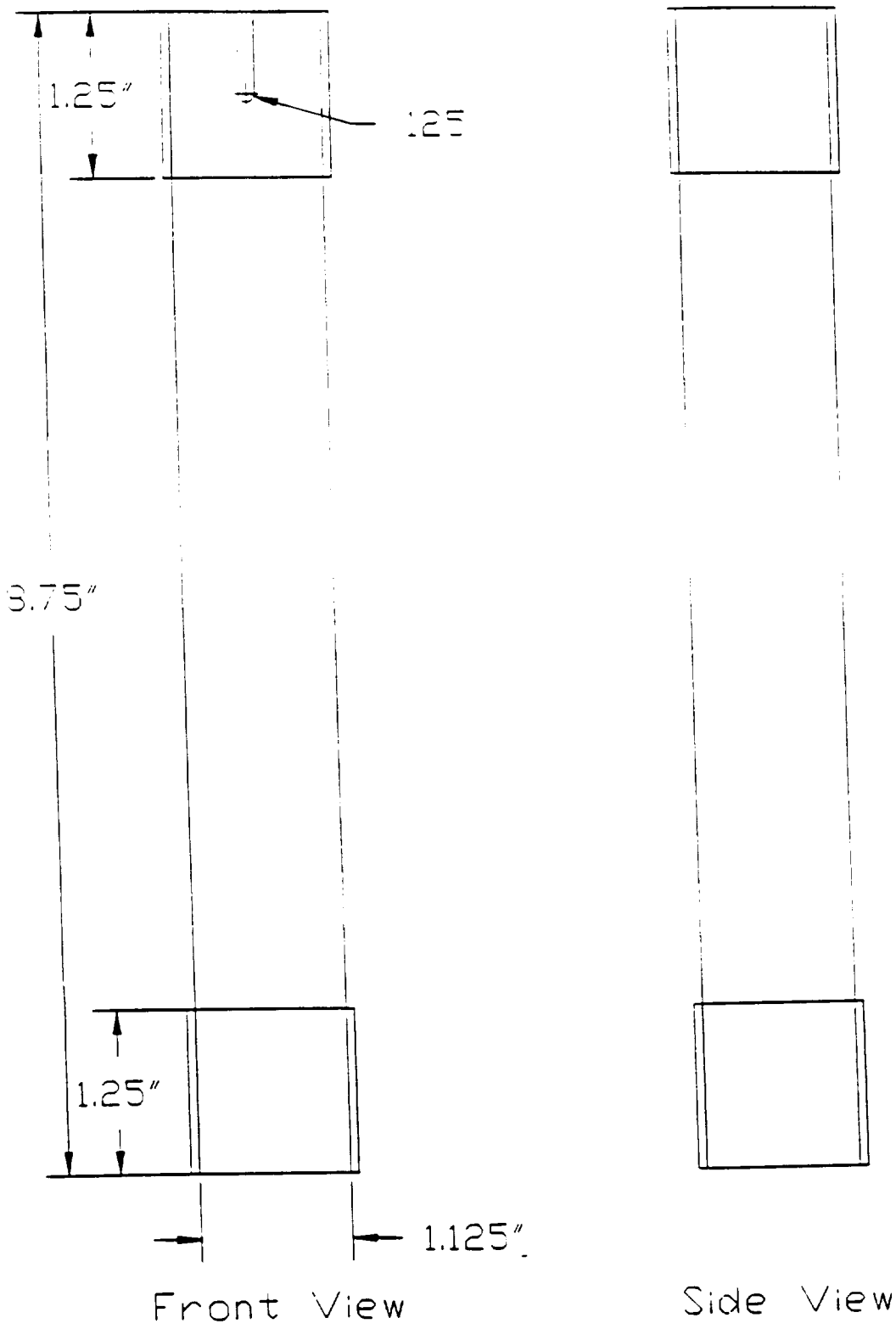

Figure 5.5 Magnetic Winding Coil Form: Front and Side View

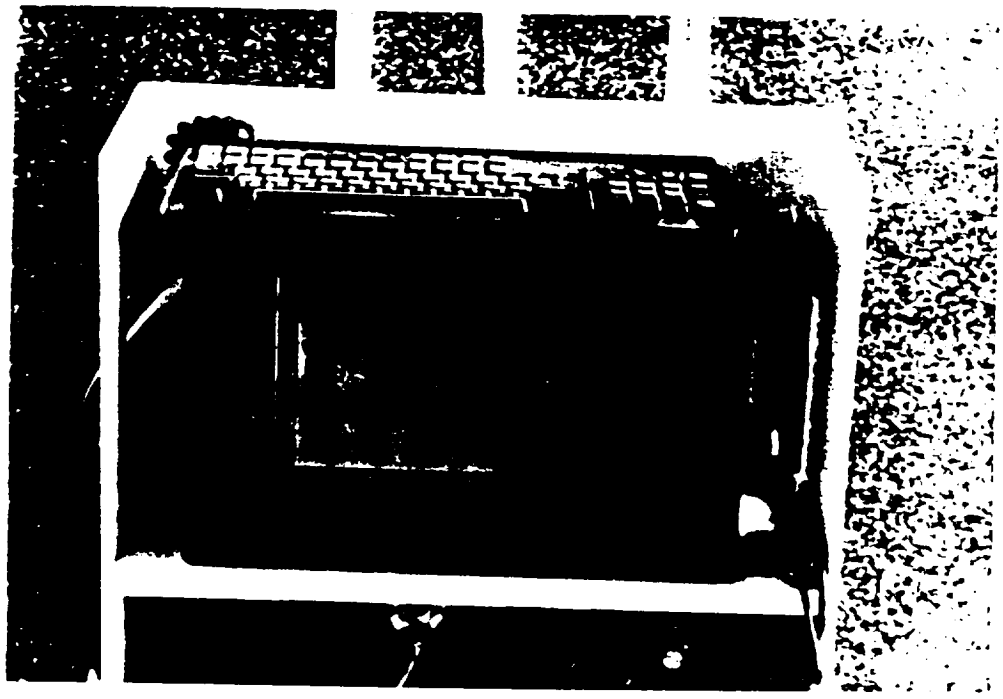

Figure 5.6 Data acquisition, signal processing, and data display was done by laptop computer shown here.

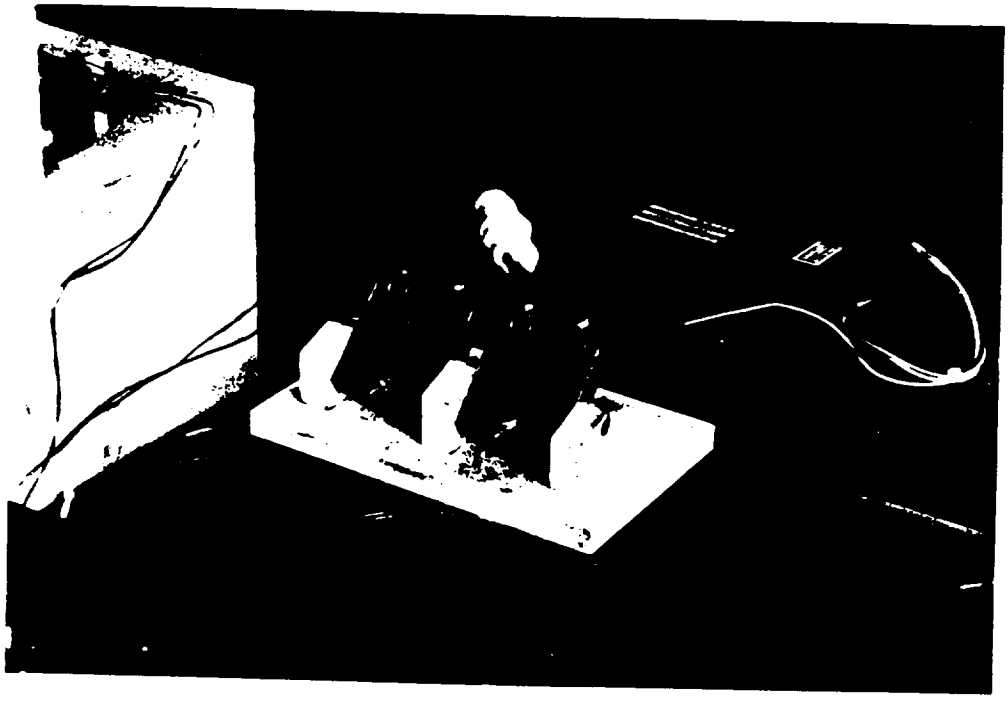

Figure 5.7 Interference fringe visibility is optimized by adjusting the polarization controllers shown here.

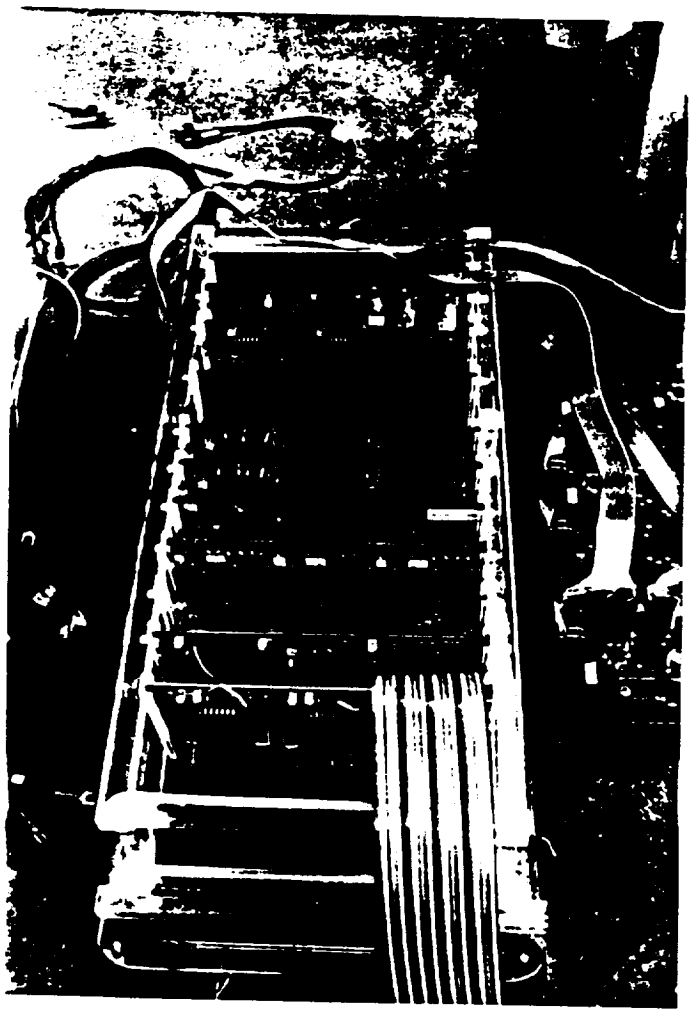

Figure 5.8 Analog electronic circuits shown here performs optical detection, feedback control, demagnetization, and filtering functions.

6.0 OPERATIONAL PROCEDURE

A step-by-step procedure is required prior to operating the instrument. These steps are listed in Table 6.1. First, the laser should be turned on by connecting the dc power supply and allowed to warm up for about one hour.

6.1 Optical Loop Set-Up

After laser thermal equilibrium is reached, the sum power level in each interferometer should be maximized without reaching saturation levels. If this value is low, the laser-fiber coupler can be tuned to produce the optimal light power. It is important to maintain the proper value because this figure contributes to the overall gain in the optical and magnetic control loops.

Next, the optical control loop parameters need to be tuned. The system can be locked by connecting the output driver to the pzt feedback element. The test pzt should now be driven with a signal generator at 100 hz. The optical feedback should be able to track this signal up to the limits of the electronics. However, in practice, only about 8 V peak-peak can be realized.

The time constant pot should be adjusted as necessary to maintain a closed loop bandwidth of 100 Hz. Once the optical loop is correctly locked, the balance point about quadrature should be adjusted. This step is accomplished by driving the interferometer at a frequency above the tracking bandwidth of the control loop. Typically, 10 KHz is used. The magnitude of this signal should be slowly increased until maximum amplitude is reached before higher order harmonics are introduced. At this value, the peak modulation has been attained. By slightly increasing the amplitude, small distortion dimples will appear. If these dimples on the top and bottom of the waveform grow asymmetrically, the balance point offset needs to be tuned. This is accomplished by adjusting the balance pot until the dimples are the same size.

Table 6.1 Steps Required to Operate 3-Axis Magnetometer

OPTICAL LOOP	COMMENT
Turn on laser	Warm up time 1 hr.
Check light power level	Adjust coupler if low
Lock optical loop	Connect feedback pot
Maintain closed loop bandwidth of 100 Hz	Adjust time constant pot
Balance interferometer about quadrature point	Adjust balance pot
Repeat for other interferometer	
MAGNETIC LOOP	**COMMENT**
Turn on x-axis dither	Use computer controller
Zero analog output	Set proper dc level on DAC
Demagnetize	Repeat until subgamma residual is obtained
Repeat for Y-Axis	
Repeat for Z-Axis	
Lock all channels	Instrument is ready for operation

6.2 Magnetic Loop Set-Up

With the optical inputs locked in quadrature, the magnetic loops can be set up. The main task involved is to demagnetize the transducers to minimize the residuals, and lock the loop.

The steps involved are as follows. The dither drive should be turned on the channel to be operated, and the magnetometer signal is nulled by adjusting the DAC offset value. A demagnetization field of 2 gauss peak value at 100 hz should be applied which rises to its maximum value in 10 sec and decays to zero in 20 sec. Usually, a residual value will remain. This offset can be nulled again by adjusting the dc offset on the DAC. The best results are achieved by demagnetizing again at half the peak field value or 1 gauss, nulling the residual field, and repeating the demag process with a .5 gauss peak field.

The other channels can be demagnetized similarly. Once the first channel has been demagnetized three times with successively smaller peak fields, the dither is turned off, and another dither is turned on. The first dither is turned off to prevent any cross-inductance effects on the gradient transducer during demag. Likewise, the third channel is demagnetized with the dithers on the first two turned off.

With all channels demagnetized three times each, the dithers should be turned on simultaneously. Demagnetization with a .2 gauss peak field is then applied to all sensors, and the residuals are zeroed. At this time, all three channels can be locked. When the feedback is activated, the transducers will be locked with a residual on each. These residuals should be less than one gamma for satisfactory operation. If either channel is locked at a substantially higher value, lower sensitivity and larger drift will result. The demagnetization process may need to be repeated.

In order to optimize the output of the magnetic transducer, careful setting of the dither frequency and amplitude is necessary. The sensitivity and drift of a closed loop sensor are dependent on these parameters.

The transducer characterization procedure begins by magnetically dithering the metglas sensor. The minimum frequency should be 5 KHz to avoid the acoustic band. As the frequency is increased up to 10 KHz, several maxima in the response will be observed. The amplitude of the dither should be reduced until only first and second order harmonics result.

This set of frequencies form the candidates for operation. Next, the transducer should be oriented perpendicular to the earth's field to null all magnetic fields. At each frequency to be tested, the transducer should be demagnetized and the residual should be recorded. The appropriate operational frequency should be the one with the smallest residual, resulting in minimum drift.

The magnetic loop is ready to be closed. The intermediate gain may require adjustment to achieve satisfactory lock. This may take several attempts.

7.0 LABORATORY NOISE TESTS

The triaxial magnetometer was operated in the laboratory to establish a crude system noise level. The laboratory noise level was independently monitored using a three axis NanoTesla fluxgate magentometer. In all cases, the laboratory noise level was found to be lower by a factor of 2-3 than the fiber optic system. Typical laboratory noise levels are lower than 1 nT rms below 1 hz.

7.1 SYSTEM NOISE

Figures 7.1a-c illustrate typical magnetometer noise runs in the laboratory. For all these cases only a single axis is active. This configuration produces the lowest operating noise level for the system. Still, considerable system noise is present. As an example, Figure 7.1d represents very quiet operation in the laboratory (in fact the nearest to the actual laboratory noise level). Figures 7.1a and 7.1b have similar higher frequency noise but both exhibit a rather large low frequency offset not associated with laboratory noise. As will be discussed later, this type of drift is believed to be caused by polarization or laser drift arising from various sources. Figure 7.1c appears to have less drift.

Figure 7.2 is a composite noise spectrum of noise data sections. The scatter in the curves is not representative of the scatter in the laboratory noise but rather of instrument performance. The laboratory noise level remained slightly below the lowest curve for the whole period. As noted above, the largest contributing factor to the scatter is the presence or absence of sensor drift during the collection cycle. This drift limits meaningful conclusions about crosstalk and cross-sensor interference because it is independent from sensor to sensor.

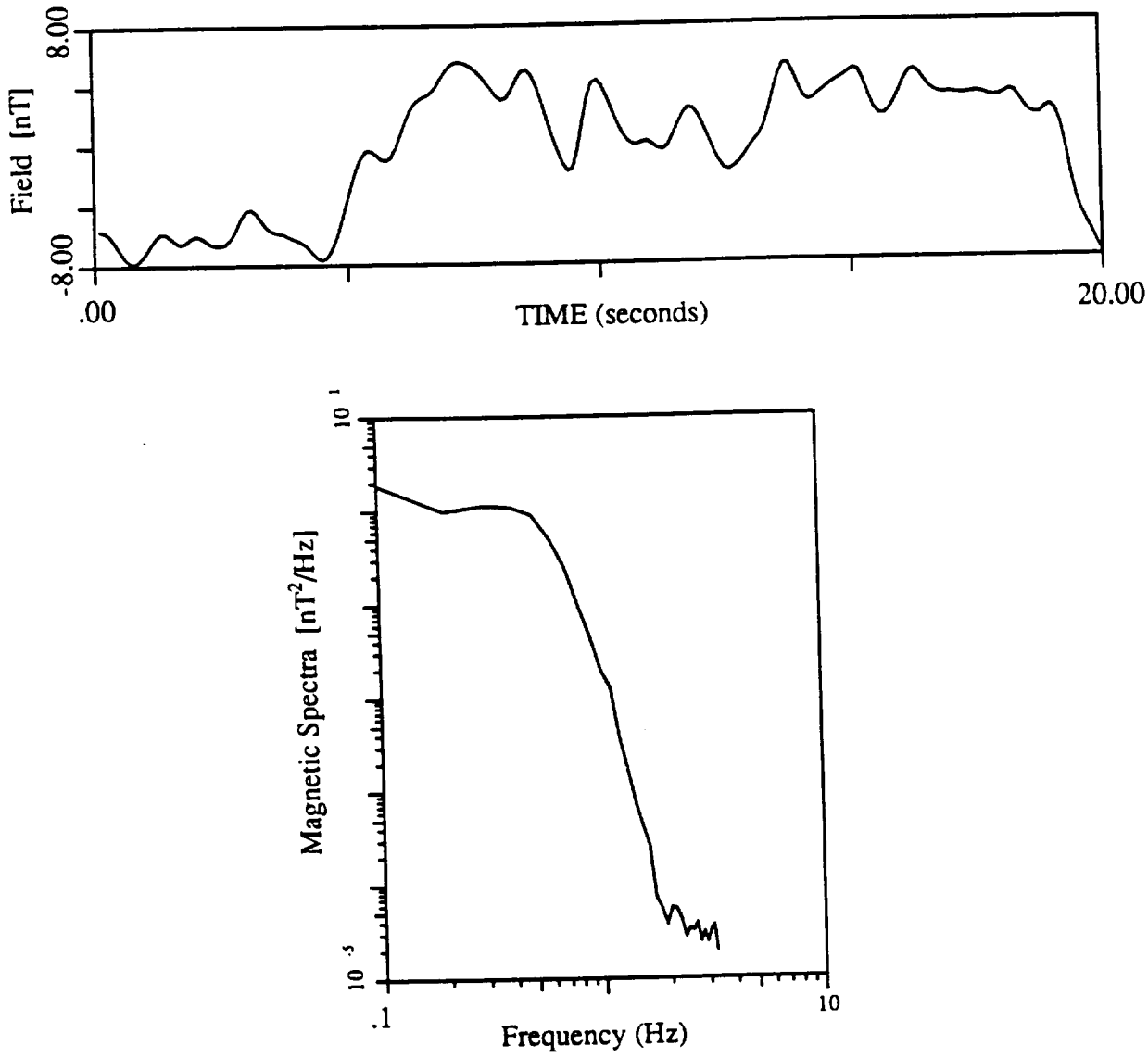

Figure 7.1 a-d Realizations of single axis magnetic noise in the laboratory. Only one channel operating with all other dithers off.

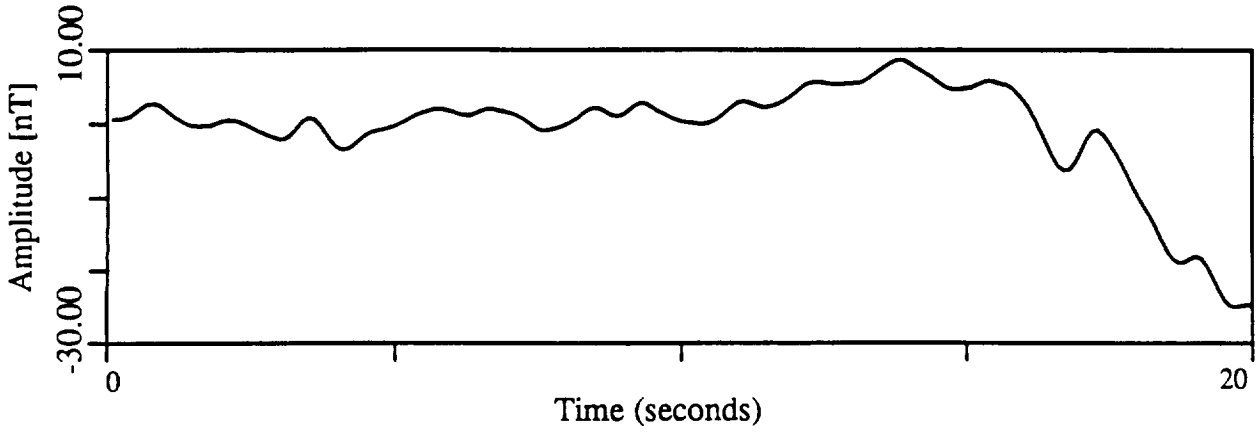
Amplitude [nT]
10.00
-30.00
0
20
Time (seconds)

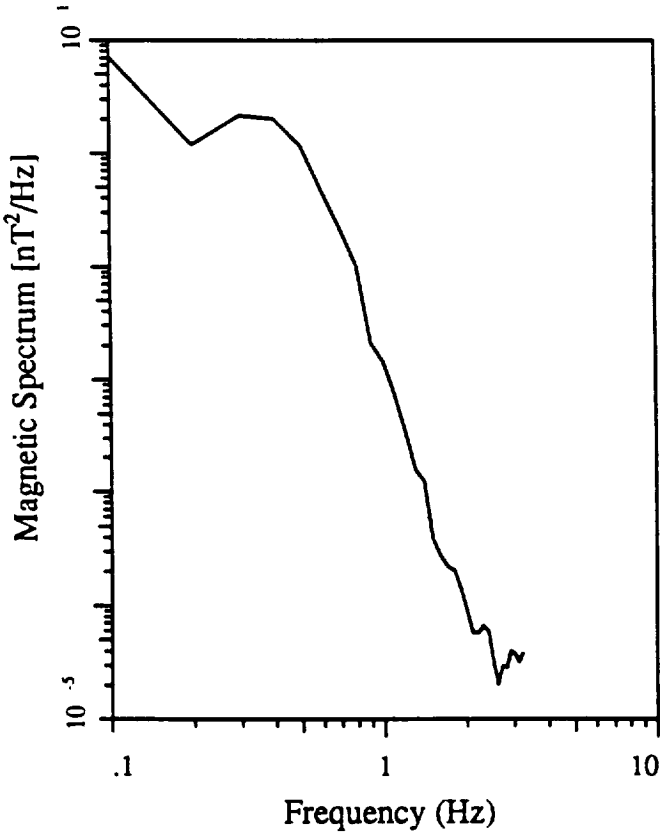
Magnetic Spectrum [nT²/Hz]
10 ⁻¹
10 ⁻⁵
.1
1
10
Frequency (Hz)

Figure 7.1b

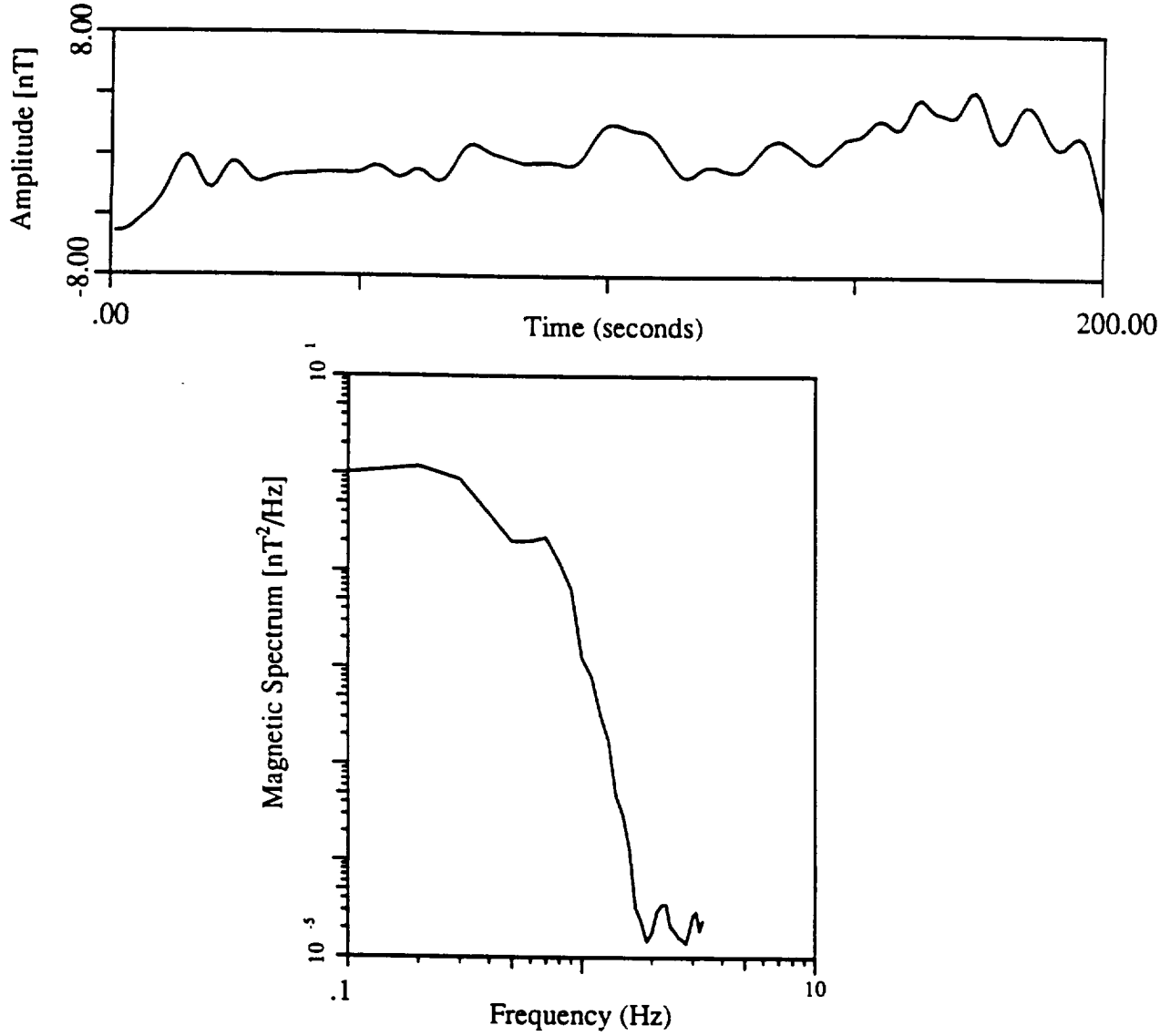
Amplitude [nT]
8.00
-8.00
.00
Time (seconds)
200.00
Magnetic Spectrum [nT²/Hz]
10 ⁻¹
10 ⁻⁵
.1
10
Frequency (Hz)

Figure 7.1 c

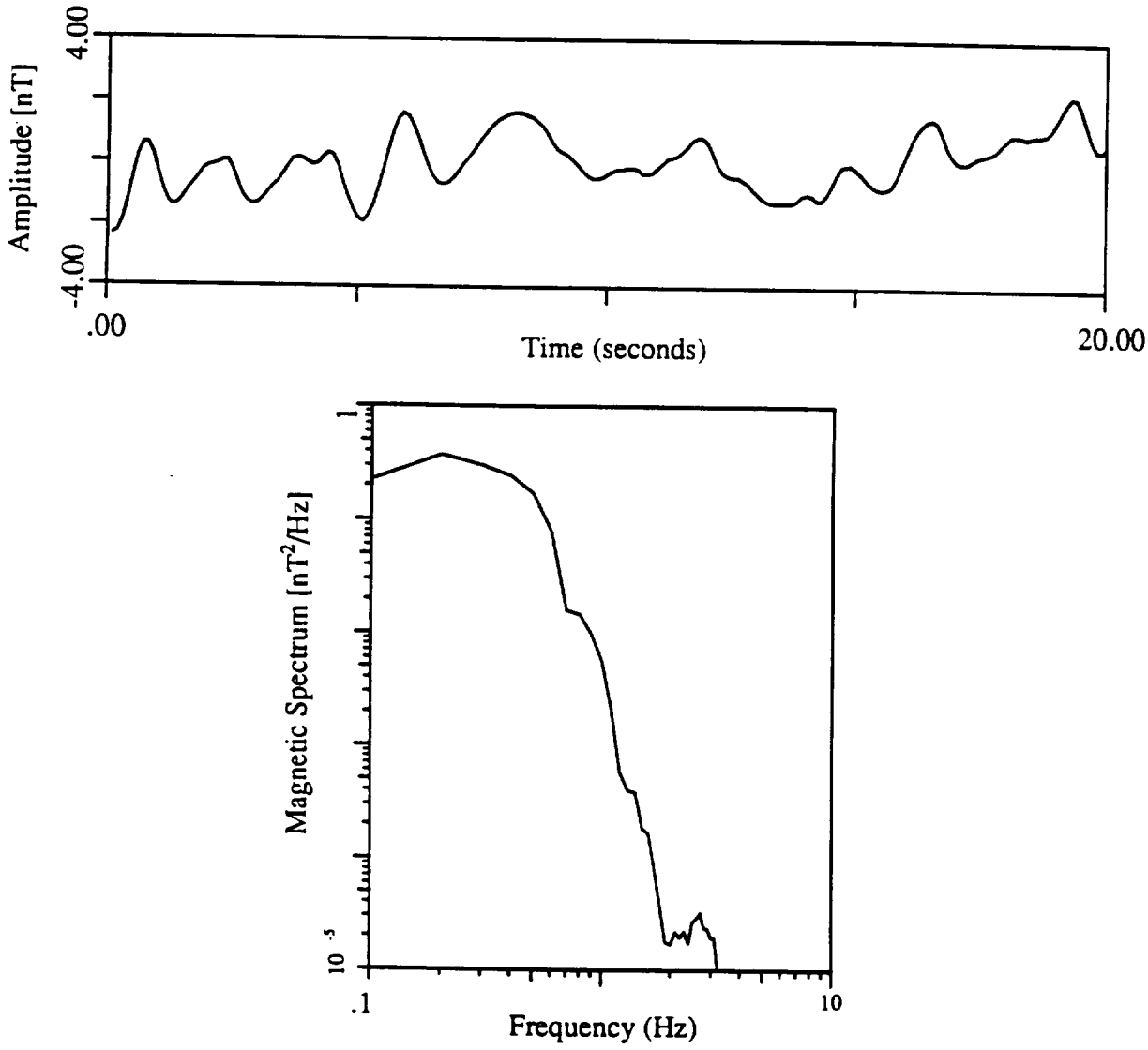
Amplitude [nT]
4.00
-4.00
.00
Time (seconds)
20.00
Magnetic Spectrum [nT²/Hz]
1
10 -5
.1
10
Frequency (Hz)

Figure 7.1 d

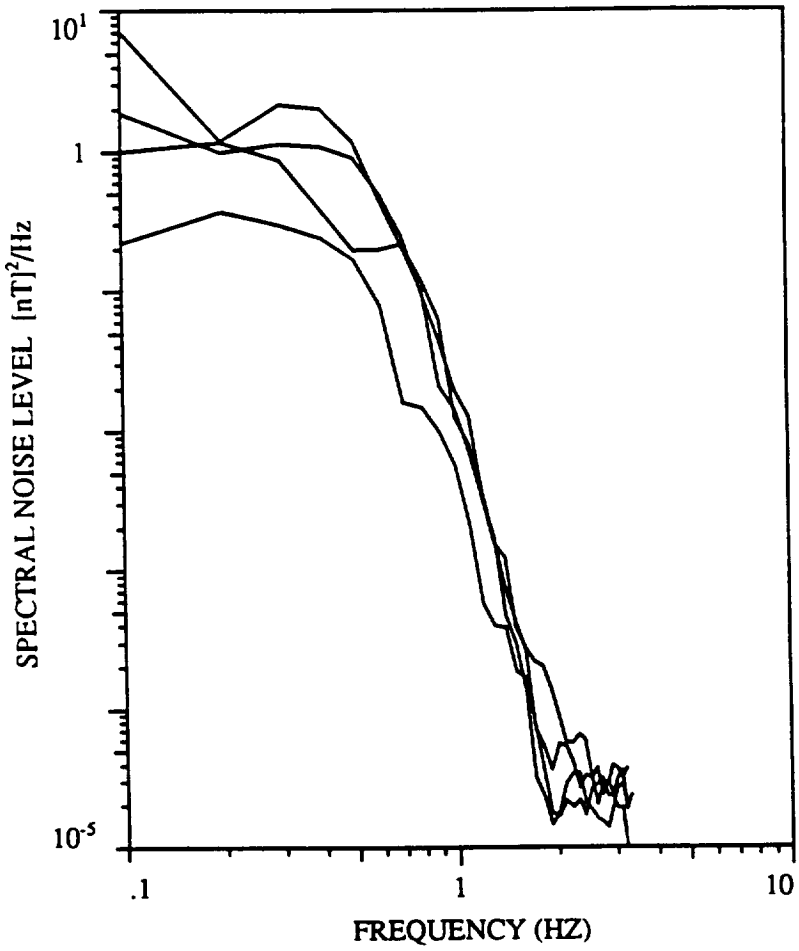

Figure 7.2 Composite noise spectrum for the magnetometer system in the laboratory environment. There is a lowpass filter applied at 0.5 Hz.

7.2 CROSS-CHANNEL INTERFERENCE

All of the above results are representative of single sensor operation. One of the biggest questions about operation of the nulling feedback system was channel to channel interference. This problem was investigated by first considering a single channel (the x-axis in this case) first operating alone, then with the dither fields on for one then two additional channels (but with the other two channels unlocked). The results of one such test is shown in Figure 7.3. The solid line, representing single channel operation, is at a typical noise level. The addition of one and then two dither fields appears to significantly raise the noise level over that achieved in single channel operation. With all dither fields operational, the noise level has risen slightly over one order of magnitude. It is possible that part of this increase in noise is due to the fact that the additional channels were not locked and hence were not at a null.

Figures 7.4 and 7.5 show operation with two and three channels simultaneously locked and operating. Figure 7.4 represents the ensemble average of four data sections for two channels operating and locked. The average is approximately one order of magnitude higher than that indicated in Figure 7.2 for single channel operation. Figure 7.5 for three axis operation has noise levels comparable to the single axis noise levels.

The above inconsistency is not well understood and may well be related to the difficulty in simultaneously locking all three channels. All three channels could only be simultaneously locked if the demagging nulling procedures were optimized for all three channels. If a bias exists on any channel, that channel will be more susceptible to noise and drift and will only be marginally locked or soon come unlocked. The increased local rf noise from multiple dithers requires better nulling than that for a single channel so better performance might be attained.

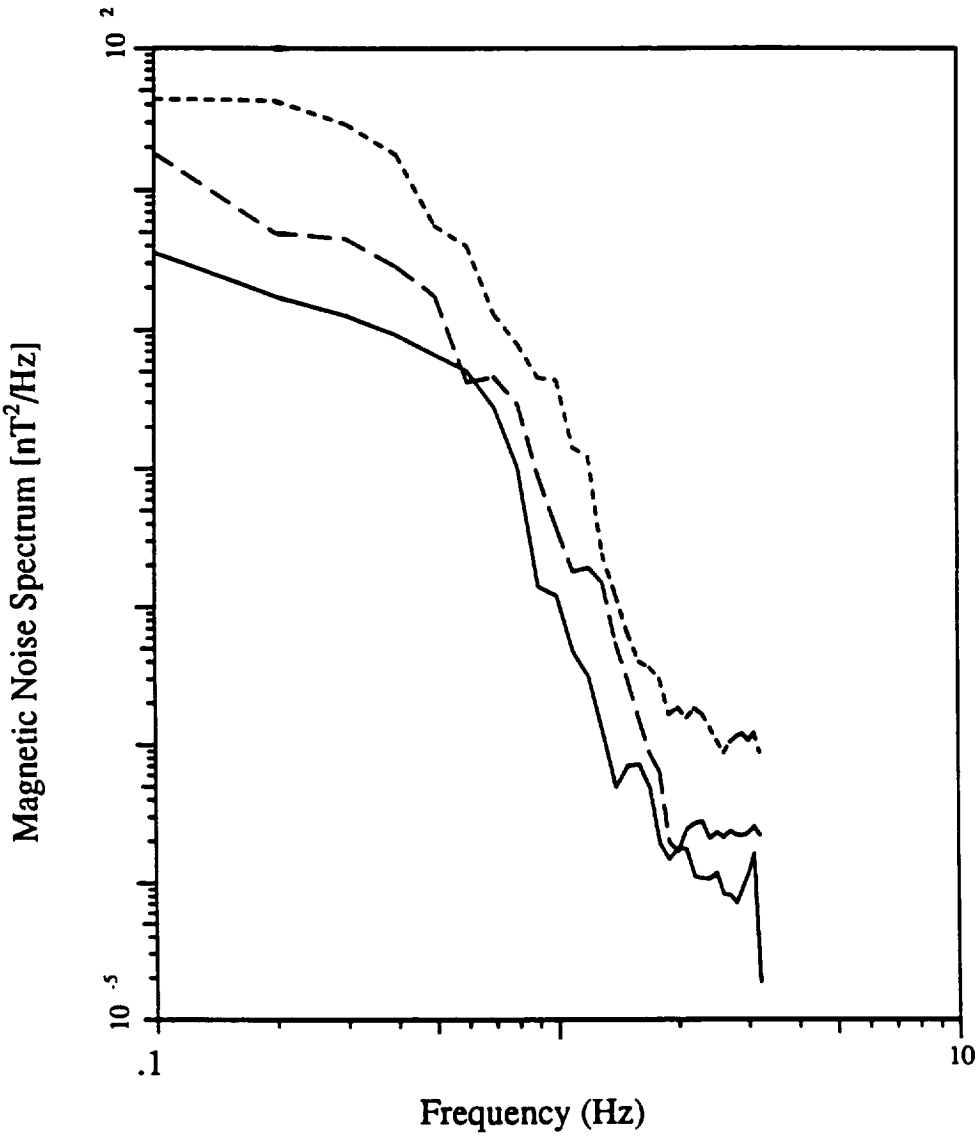

Figure 7.3 Comparison of the single channel noise levels with the dither fields on but the other channels not locked. Solid curve is with no additional channels operating; dashed curve is with one dither on; dotted curve is with two dither fields on.

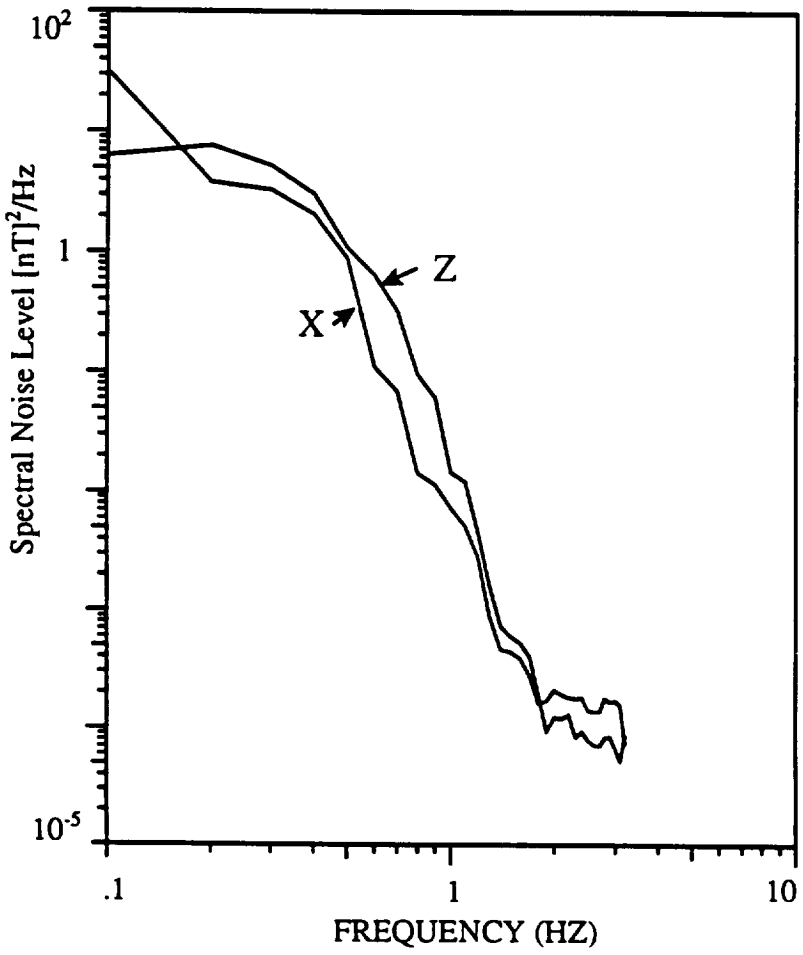

Figure 7.4 Noise spectra for the X and Z channels locked and operating simultaneously.

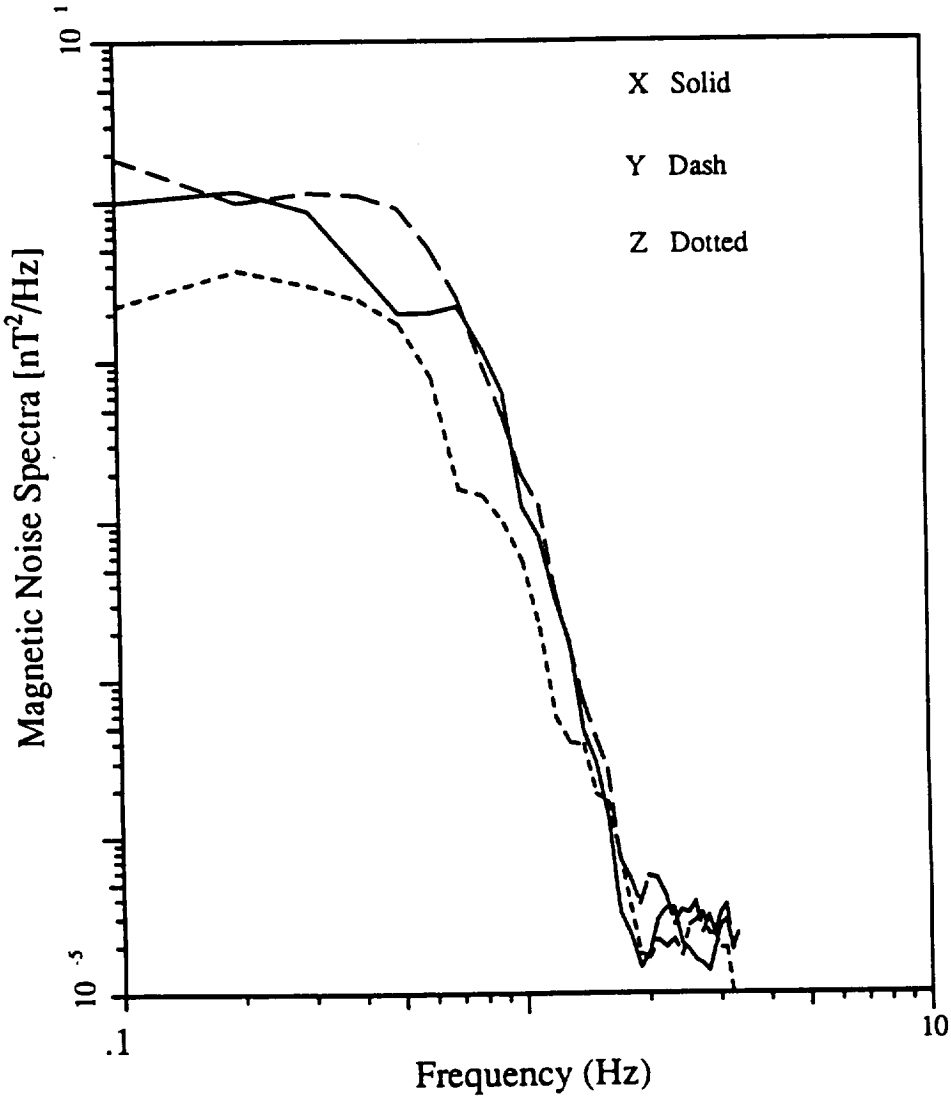

Figure 7.5 Three axis noise levels with all channels locked and operating.

As will be discussed later, the demagnetization procedure, although relatively automated, does not appear to be consistent from try to try or from channel to channel. Even attempts to exactly repeat a demagnetization procedure resulted in varying levels of residual bias (and thus drift levels). No solution to this problem was found, possibly because it may be driven by the variability in the transducers themselves. Factors contributing to noise will be discussed further in the next section.

8.0 NOISE SOURCES

Any strain induced in the sensor section of the optical fiber will produce an output in the interferometer that is indistinguishable from a signal in the same frequency band. In this regard the two most common noise sources are temperature variations and structural vibration, as indicated by a typical laboratory noise interferometer spectrum (Figure 8.1). Low frequency temperature fluctuations are still likely to exist, but the signal processing technique described in Section 2 should place the upshifted magnetic signal in the sensor noise limited range of frequencies (~1 kHz).

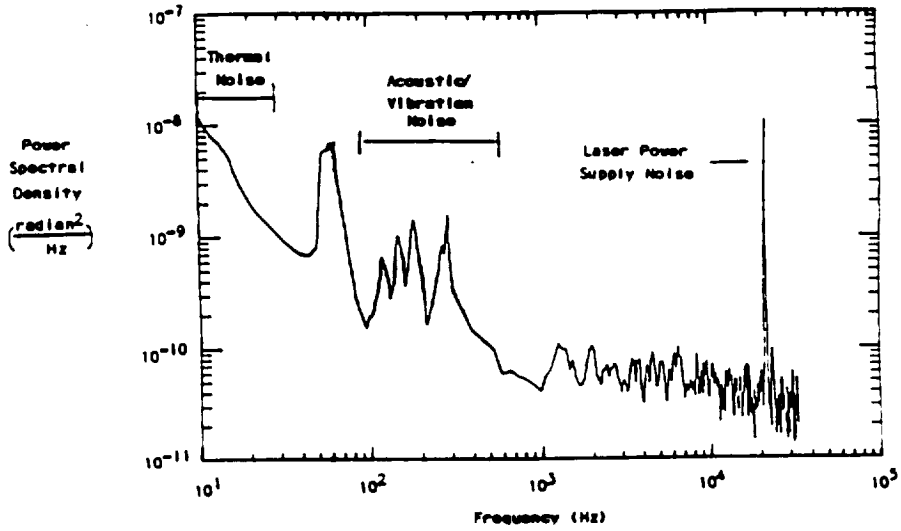

Figure 8.1 Laboratory Noise Interferometer Spectrum

8.1 Interferometer Drift

The He-Ne laser frequency drift with temperature, coupled with the large path length imbalance in the test interferometer, causes a feedback voltage drift. The size of the feedback voltage drift, δV_f, associated with a drift in the laser frequency of δf is given

by

$$\delta V_f = \left[\frac{2\pi n (L_1 - L_2)}{cK_f}\right] \delta f \qquad (8.1)$$

where (L_1-L_2) is the path length mismatch between the two arms of the interferometer, c the free space velocity of light, and the other symbols as defined previously. Using the values $(L_1-L_2) = 40$ cm, $n = 1.447$, $c = 3.00 \times 10^8$ m/sec., and $K_f = 17.26$ rad./volt we obtain the value $\delta V_f/\delta f = 7.1 \times 10^{-10}$ volts/Hz. The laser frequency shift can be produced by a change in the laser cavity length L_c, due to small changes in the laser temperature. This can be seen by noting that the wavenumber of the mth cavity mode is given by

$$k_m = \frac{m\pi}{L_c} = \frac{2\pi f}{c} = \frac{2\pi}{\lambda_o} \qquad (8.2)$$

so that the frequency shift of the mode is

$$\delta f = - \frac{c}{\lambda_o} \left[\frac{\delta L_c}{L_c}\right] \qquad (8.3)$$

Assigning an effective linear thermal expansion coefficient α, such that

$$\frac{\delta L_c}{L_c} = \alpha \delta T \qquad (8.4)$$

where δT is the temperature change of the laser tube, we obtain the laser frequency shift with temperature

$$\delta f = - \frac{c}{\lambda_o} \alpha \delta T \qquad (8.5)$$

Taking the conservative estimate for the expansion coefficient of $10^{-6}/^{o}C$ (Pyrex is $3.2 \times 10^{-6}/^{o}C$), and $\lambda_o = 6.33 \times 10^{-7}$ m, we obtain the value of $\delta f/\delta T = 4.7 \times 10^{8}$ $Hz/^{o}C$. Combining (8.1) with (8.5), we obtain for the feedback voltage change with laser temperature fluctuation,

$$\delta V_f = - \left[\frac{2\pi n (L_1 - L_2)}{\lambda_o K_f} \right] \alpha \delta T \qquad (8.6)$$

Using the above values we obtain $\delta V_f/\delta T = .34$ volts/^{o}C. The feedback voltage is extremely sensitive to laser temperature and interferometer path length imbalance. Equation (8.5) is only valid over relatively small temperature deviations, certainly no more than the temperature deviation required to produce a frequency shift as large as the cavity mode spacing, at which point the next laser cavity mode shifts under the gain curve and replaces the original lasing mode. Equation (8.6) shows the virtue of path length matching the interferometer arms.

Thus we see that with a 40 cm path length imbalance of the testbed interferometer, a $0.03^{o}C$ laser temperature change causes a 10 mV change or drift of the PZT feedback voltage. This magnitude of temperature drift is easily caused by air currents, as the laser tube was not actively thermally stabilized. This hypothesis was verified experimentally in two ways. First, the laser tube was slightly cooled by gently placing a hand on the outside of the laser tube momentarily. After about 15 seconds, the feedback voltage began to drift several volts in one direction and returned slowly to near its initial value after the hand was removed. To see if air currents could cause drift of the observed magnitude, a can of dry air was sprayed gently on the outside of the laser tube for about 10 seconds. This caused the PZT feedback voltage to drift rapidly and reset every few seconds. Thus it was established that small laser temperature fluctuations, coupled with the large path length mismatch of the test interferometer, were responsible for the DC drift, and <u>not</u> temperature fluctuations of

the arms of the interferometer. (The test interferometer was housed in a plastic box, and the external transducer leads in plastic cable, except for a few feet of exposed, acrylate-only coated fiber.)

Along these lines, the path length imbalance can easily be reduced to less than one centimeter, thus giving a factor of at least 40 improvement in the DC drift due to laser temperature fluctuations according to Equation (8.6). In addition, an appropriate low cost laser with excellent provisions for active temperature control is commercially available, and this should greatly improve the laser frequency stability. It is conservatively expected that these two improvements will result in at least a factor of 100 reduction of residual DC drift in the interferometer.

8.2 RADIATION

Radiation is also a potential environmental noise source. The effect of radiation is to increase the transmission loss in the fiber and thereby reduce the optical signal-to-noise ratio at the detector for a shot noise limited system. Most fiber darkening is transient in nature, with the recovery time depending on the dose rate, the total dose, the fiber temperature, and the fiber material composition. Figure 8.2 illustrates an initially rapid reduction in transmission that increases more slowly with time, depending on the temperature. (The curves for $0^{o}C$ and $30^{o}C$ are most appropriate to the spacecraft application.) The fiber is observed to "recover" exponentially, but not necessarily to its virgin condition.

The effect of dose rate is illustrated in Figure 8.3, where for a fixed total dose of 400 krad, higher dose rates result in greater radiation induced loss. However the recovery rate is also faster for higher dose rates (Figure 8.3). While the total doses are much higher than the 50 krad noted in the benchmark specifications, a conservative design approach would be to provide about 10 dB power margin above shot noise limited operation.

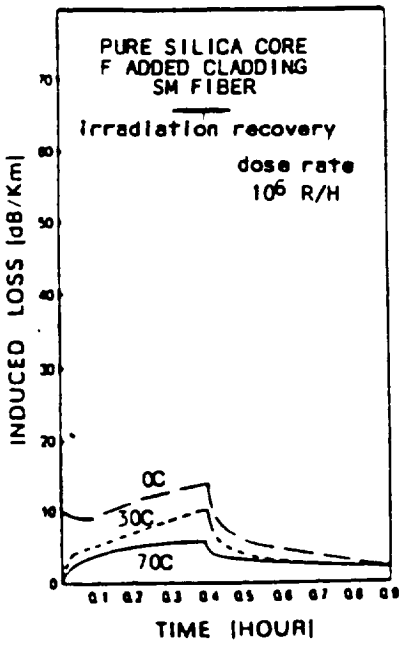

Figure 8.2 Radiation-induced Loss vs Time in Pure Silica Core F Added Cladding SM Fiber as A Function of Temperature During and Following Exposure to $4x10^5$ rad

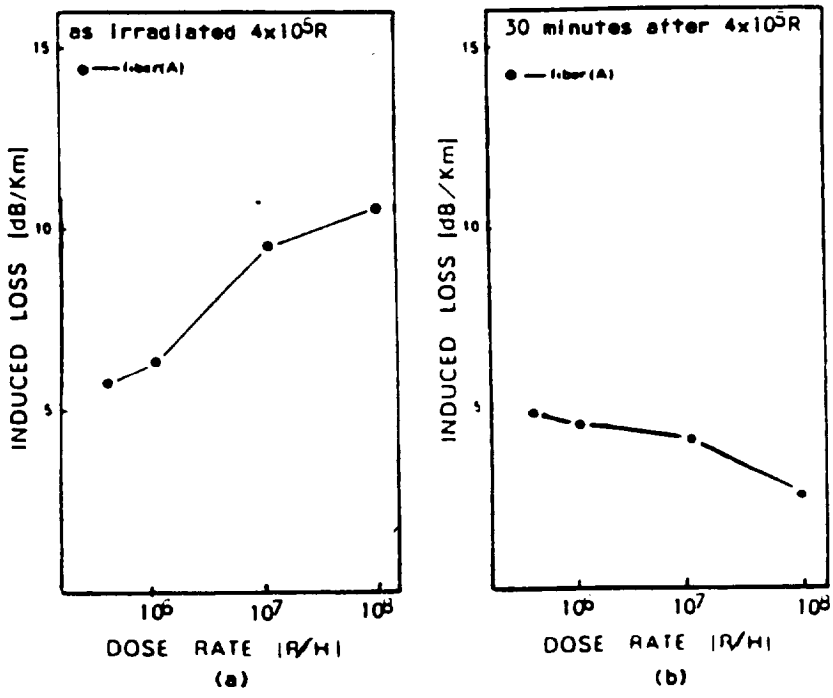

Figure 8.3 Radiation-induced Loss of (a) Just After and (b) 30 Minutes after Exposure to $4x10^5$ rad in Pure Silica Core F Added Cladding SM Fiber as a Function of Dose Rate

For an interferometer, the phase equivalent shot noise is

$$\phi_s^2 = \frac{h\nu B}{P_d}$$

where h is Planck's constant, ν is the optical frequency (Hz), B is the detection bandwidth (sec^{-1}), and P_d is the required power on the detector. For a system with 1 μrad shot noise and a 10 Hz bandwidth, the required power on the detector $P_d \simeq 2$ μW. Therefore, a conservative design should provide about 20 μW at the detector; a readily achievable criterion.

8.3 Effect of Polarization Fade

The polarization of the light in the transducer and reference legs of the interferometer sensor may drift with respect to one another during instrument operation. These polarization shifts cause interference fringe visibility fade which results in loss of instrument sensitivity and signal-to-noise ratio.

The fiber used in the present three axis magnetometer has no polarization preserving properties. Thus, small environmental and mechanical perturbations may alter the birefringence state of each fiber leg enough to cause polarization drift. Understanding the effect of random external factors on the system output may be simplified by assuming that the polarization in the signal and reference legs are uncorrelated and that they drift randomly.

8.3.1 Sensitivity Fade

The outputs I_1 and I_2 of the fiberoptic interferometer locked in quadrature have intensity values given by

$$I_1 = I_o(1 + m\sin\theta_s) \quad (8.1)$$

$$I_2 = I_o(1 - m\sin\theta_s) \quad (8.2)$$

where I_o = total interferometer light power
m = fringe visibility $0 < m < 1$
θ_s = induced signal phase shift

The fringe visibility m is unity when the polarization states of the light in each leg are identical, and m is zero when the polarization states are orthogonal.

The normalized phase sensitivity to small signals is given by

$$S = | m | \quad (8.3)$$

Given a minimum sensitivity level S_0, it can be determined the probability P that S is greater than S_0.

The state of polarization of the light in each arm of the interferometer can be represented by a unit vector on a Poincare sphere, where each vector extends from the center of the sphere to a point on the surface. Suppose the input polarization state at the output coupler is given by η_S, for the signal arm, and η_R, for the reference arm. Then the mixing efficiency is given by

$$m = \cos(\phi/2) \quad (8.4)$$

where ϕ is the angle between the unit vectors.

Given the assumption that temperature and mechanical fluctuations cause the polarization state of each interferometer arm to drift randomly, the unit vectors η_S and η_R are allowed to wander randomly around the surface of the Poincare' sphere. This condition is equivalent to the position of the unit vectors η_S and η_R having a uniform probability distribution over the surface of the sphere.

Thus, the probability that the polarization vectors η_S and η_R have an angle less than some angle ϕ is calculated from the ratio of the spherical cap subtended by the unit vector η_R at angle ϕ over all angles θ to the area of the entire sphere. This probability is given by

$$P = 1 - \cos^2 (\phi/2) \qquad (8.5)$$

The fringe visibility factor m, hence the interferometer sensitivity, depends on the angle ϕ between the polarization vectors.

8.3.2 Signal-to-Noise Ratio Fade

In the gradiometer instrument, the signals of interest are the low frequency magnetic signals upshifted in frequency by the dither. As the polarization fades, the signal to noise ratio will also decrease. The signal fade will reduce the effect of environmental and instrument noise with respect to photodetector shot noise.

The photodetector current i_p is proportional to the optical intensity given in (8.1).

$$i_p = K\,(1 + m\sin(\theta_s + \theta_n + \theta_S)) \qquad (8.6)$$

where K is a proportionality constant.

The photodetector sees two terms, θ_S and θ_n, the signal phase and the noise phase shift from environmental and instrument sources. However, an additional shot noise term θ_S comes in at the photodetector output. For the signal θ_S term, the mean square signal current from (8.5) is given by

$$i_s^2 = K^2 m^2 \theta_s^2 \tag{8.7}$$

For the noise θ_n term, the mean square noise current is the sum of the environmental and instrument noise. The shot noise from the photodetector has a bandwidth B and electronic charge e.

$$i_n^2 = K^2 m^2 \theta_n^2 + KeB \tag{8.8}$$

The signal-to-noise ratio is given by

$$\frac{i_s^2}{i_n^2} = \frac{K^2 M^2 \theta_S^2}{K^2 M^2 \theta_n^2 + KeB} = \frac{\theta_s^2}{\theta_n^2 + \frac{eB}{KM^2}} \tag{8.9}$$

In practice, the environmental and instrument noise θ_n is much larger than the shot noise term θ_S. However, polarization fade will reduce both the θ_S and θ_n terms in which enhances the shot noise term θ_S, resulting in a decrease in the signal to noise ratio.

Thus, for improvement in the instrument sensitivity and noise rejection capabilities, control of polarization fade is very important. Random drift in polarization may be caused by thermal and environmental sources leads to loss in instrument sensitivity and signal-to-noise ratio. One possible solution is to use polarization preservation fiber to prevent fading. Also, by placing the fiber in the transducer and reference legs together along the entire length of the interferometer, polarization drift in the two legs may be correlated, thus preventing a complete fade condition. Finally, automatic polarization control techniques may be used, but system complexity would be increased.

9.0 RECOMMENDATIONS FOR FUTURE RESEARCH

Major advances were made during Phase II toward developing a deployable high performance fiber optic vector magnetometer. Compact, low-noise optical and electronic subsystems were developed, along with a well characterized near-optimized transducer. However, two key problems were encountered that precluded the immediate transfer of the current technology to a deployable system. These are:

- Low frequency drift associated with the laser source and/or fiber polarization

- Apparent variability in transducer characteristics at very low fields over extended periods.

It was not possible to resolve these problems within the scope of the Phase II program. We believe the first problem could be addressed successfully by the use of polarization preserving fiber together with new narrow band stable laser diodes being researched for the fiber optic communications industry. The second problem may require more fundamental research on the material characteristics of metallic glass and the detailed influence of various fabrication techniques. Some of this type of research has been continuing at the Naval Research Laboratories, but major breakthroughs have not occurred at this writing.

We believe the concept of a fiber optic magnetometer is still very promising, pending the results of engineering and materials research. Much progress has been made, but we are not prepared to extend the program until specific approaches have been identified for resolving the current technical issues.

10.0 REFERENCES

1. T.D. Wang, D.G. McComb, B.R. Kingston, K.H. Wanser, K.A. Poehls, M.C. Dube, "Portable Fiber-Optic Vector Magnetic Gradiometer for Buried Ordnance Detection," Dynamics Technology Report DT-8619-89006, October 1989.

2. C.M. Dube, S. Thordarson, K. H. Wanser, "Fiber-Optic Magnetic Gradiometer," Dynamics Technology Report DT-8507-02, July 1987.

3. D. W. Stowe, D. R. Moore, R. G. Priest, "Polarization Fading in Fiber Interferometric Sensors," IEEE Transactions on Microwave Theory and Techniques, Vol. MTT-30, No. 10, October 1982.

4. K. H. Wanser, T. D. Wang, "Interferometric Measurement and Calibration of DC Strain of a Fiber Optic Embedded Graphite Epoxy Composite Panel," Proceedings of SPIE 1170, 1989.